Development of Highly Stable Lamella Using Polyelectrolyte Complex Nanoparticles: An Environmentally Friendly scCO₂ Foam Injection Method for CO₂ Utilization Using EOR

^{1,2}Negar Nazari, ¹Hooman Hosseini, ³Jyun Syung Tsau, ³Karen Shafer-Peltier, ^{4,5}Craig Marshall, ⁶Qiang Ye, ¹Reza Barati Ghahfarokhi*

¹Department of Chemical and Petroleum Engineering, University of Kansas, Lawrence, Kansas 66045, USA

Correspondence to: Reza Barati Ghahfarokhi (E-mail: reza.barati@ku.edu)

ABSTRACT

CO₂ foam flooding is a proven technology that enhances oil recovery and geological storage by improving the mobility of the injected CO₂ in depleted reservoirs. Surfactant drainage, disintegration and rock adsorption have long affected the stability of CO₂ foams in saline formations. To generate a more stable foam front in the presence of crude oil and to overcome the capillary forces destabilizing the foam lamella, polyelectrolyte complex nanoparticles (PECNP) conjugated with surfactant oligomers are introduced to the lamella generated by an aqueous phase containing high salinity to improve the EOR performance and produced water compatibility of supercritical CO₂ (scCO₂) foams. The formation of vesicular structures containing electrostatically hinged complexes of PECNP and surfactant was verified via transmission electron microscopy (TEM) while the structural changes associated with molecular complexation were identified using Raman spectroscopy. Accordingly, optimized ratios of PECNP:surfactant were employed to generate the most stable scCO₂ foam in high salinity produced water and improve the recovery of the foam flooding process. The effect of PECNP-conjugated surfactant on stability, durability, and interfacial properties of scCO₂ foam were examined. A set of core-flooding experiments in a wide range of salinity proved the capability of scCO₂ foam systems enhanced using PECNP-surfactant

²Department of Energy Resources Engineering, Stanford University, Stanford, CA, 94305, USA

³Tertiary Oil Recovery Program, University of Kansas, Lawrence, Kansas 66045, USA

⁴Department of Geology, University of Kansas, Lawrence, Kansas 66045, USA

⁵Department of Chemistry, University of Kansas, Lawrence, Kansas 66045, USA

⁶Institute for Bioengineering Research, University of Kansas, Lawrence, Kansas 66045, USA

to offer the highest apparent viscosity and incremental oil recovery. A variety of injection scenarios tested on oil-saturated limestone core samples indicating that the highest incremental oil recovery and the lowest residual oil saturation are achieved by prioritizing PECNP:surfactatnt scCO₂ foam flood in optimized electrolyte concentrations.

KEYWORDS: "Enhanced Oil Recovery", "CO₂ foam", "polyelectrolyte complex nanoparticle", "foam stability", "produced water", "CO₂ storage".

1. INTRODUCTION

The Paris Climate Accord aims at holding global temperature rise to well below 2 °C for this century by limiting greenhouse gas emission into the atmosphere [1]. CO₂ emission from power plants and industrial facilities is widely regarded as major contributor to global warming and rising global temperature [2]. However, fossil fuels still play a dominant role in global energy sector, global oil production has increased to more than 2.5-fold over the last 50 years, and crude oil has become the largest energy source on planet, accounting for around 39% of fossil energy [3]. To reduce detrimental environmental impacts of anthropogenic CO₂ emissions, various technologies for CO₂ storage have been proposed [4–6]. Compression, injection and partial storage in geological formations with the purpose of EOR is a viable approach in oil recovery from subsurface resources [7–9].

CO₂-enhanced oil recovery (EOR) is introduced as a promising tool for greenhouse gas emission reduction [10], since a CO₂ capture process from industrial facilities can provide the anthropogenic CO₂ required to inject and store in geological formations and to enhance the production [11]. Therefore, CO₂ for oil production with associated storage can reduce environmental impacts and contribute to Carbon Capture, Utilization, and Storage (CCUS) [12]. The US Department of Energy (DOE) has long been investing in next generation of CO₂-EOR research for production and sequestration [13]. Accordingly, successful storage of CO₂ in geological formations have been reported across the US [8]. Additionally, CO₂ injection has been used to improve the recovery of oil reservoirs since the 1950s [14]. CO₂ miscible flooding, performed at reservoir pressures higher than the minimum miscibility pressure (MMP), results in a higher microscopic efficiency [15]. However, several issues were reported with CO₂ injection such as unfavorable mobility ratio, viscous fingering, gravity override and poor sweep efficiency [10,16,17]. Bernard and Holm initially presented CO₂ foam as an effective mobility control agent with selective mobility reduction, to improve the sweep efficiency of EOR processes [18].

Supercritical CO₂ as compressed CO₂ at extreme conditions (31.1 °C and 7.4 MPa [19]) is known as a potential candidate for CO₂ storage with properties such as improved mass transfer and increased selectivity [20]. Foam offers the capability of mobility reduction where the foam quality lies between 45 to 90% [21,22]. Aqueous based scCO₂ foam is a colloidal dispersion consisting of scCO₂ in water or brine and foaming stabilizers [23]. Contributing fluids give rise to the final viscosity of foam [24], eliminate pore plugging in formation [25], lower water-usage in water sensitive formations [23], and introduce a recyclable and eco-friendly approach with aqueous phase [26].

Typically, a large quantity of water (brine) injection accompanies CO₂ floods, leading to isolation of oil from CO₂ in the reservoir [27] and excessive produced water discharge on the surface [28]. Disposal, treatment and re-use are suggested techniques to handle the large volumes of produced water from oil fields [23,29–31]. Re-injection of produced water into the reservoir is the most optimized and ecofriendly approach to handle the produced water [32]. The water involved in this process can be re-injected to create a sustainable process and to prevent excessive fresh water usage and waste water disposal [28] as injection of recyclable fluids helps to create sustainable oil production cycle for non-hazardous energy-water nexus [33].

Carbonate reservoirs account for over 60% of the world's oil and gas reserves with average recovery of less than 40% [34] opening the door to examine the potential of advanced materials such as high internal phase emulsions for energy production. The stability of the surfactant generated CO₂ foam in the presence of crude oil is a determining factor in sweep efficiency and oil recovery [35] and ultimately underground CO₂ storage [36] as spreading oil into the foam lamellae destabilizes the CO₂-water lamella interface [20]. Aqueous based CO₂-EOR requires development of CO₂-philic surfactants not sensitive to water medium for effective CO₂ mobility control in porous media [37]. Injection strategies were previously introduced with dissolution of surfactant in CO₂ [37], and better recovery was achieved when water is not injected. Conventional surfactants such as alpha olefin sulphonates are usually missing CO₂-philic functional groups such as aliphatic/aromatic branches and methylene groups [38]. Non-ionic branched nonylphenol ethoxylate or tridecyl alcohol ethoxylate surfactants with variable ethylene oxide (EO) repeating units such as Huntsman SURFONIC® N-120, N-150 and TDA-9 are increasingly used for mobility reduction due to brine soluble/CO₂ soluble properties in high pressure [17,39,40].

Despite the advances in surfactant/foam EOR in recent years [41], the stability, excessive adsorption on the rocks [42] and imbalanced head/tail solubility in CO₂/aqueous phase impacts the resulting emulsion stability achieved by surfactant generated foams [23]. Moreover, adsorption of the oil by the porous media changes the wettability of the rock and negatively affects the foam generation and regeneration [21]. Polyelectrolytes with electrostatic conjugation to the surfactants are considered promising additives for alternation of surfactant concentration [43], foam film stability [43,44] and lowering the surface elasticity [44].

Polyelectrolyte complex nanoparticles (PECNP) were originally developed for drug delivery applications [45] and due to biocompatibility to organisms were adapted to oil field applications [46,47]. Polyethyleneimine is a water soluble, non-viral gene delivery polymer that offers high transfection efficiency both in vitro and in vivo [48]. To decrease the toxicity due to polycationic activity of PEI, a degradable polyanionic Dextran sulfate (DS) is added to decrease the cytotoxicity of DNA-incorporated nano-gel [48]. Dextran sulfate is a biodegradable polymer containing a branched chain of anhydroglucose unites with 2.3 sulfate groups per glucosyl residue frequently used on pharmaceutical applications with proven biocompatibility [48]. In terms of functional properties to protect the ecosystem in oil and gas industry, Polyethylenimine-dextran sulfate polyelectrolyte complexes are used to protect the enzymes from harsh conditions and their vesicle loaded with enzymes helps to degrade the guar gels, HPG solutions and borate-cross-linked gels at variety of pH and temperature and also to degrade the filter cake therefore preventing the fluid loss in hydraulic fracturing [49]. The similar bio/organism-compatibility is expected in EOR application.

Recently, our group developed ionic nanoparticles in form of polyelectrolyte complex nanoparticles (PECNP) as stabilizers for the surfactant generated scCO₂ foam in the presence of crude oil [20,28,50,51]. Kalyanaraman and coworkers [50] improved the stability of scCO₂ foam in 2% KCl brine with a lamella mixture containing surfactant and PECNP. Results suggested improved oil recovery and sweep efficiency in subsurface CO₂ flooding with low salinity brines. Nazari et. al. [28] investigated the performance of developed foam system in various salinities of produced water. Determining the rheological property, the stability, and durability of the foam with and without the presence of crude oil showed that foam stability and durability deteriorated when water salinity increased. However, with the addition of polyelectrolyte and PECNP to the

system, the foam stability and durability was improved even in high salinity water with or without the presence of crude oil [28].

Hosseini et al [20] introduced a mechanistic study of zwitterionic surfactants and PECNP complexation in high salinity brines to lower the fluid loss and improve the fracture conductivity and production in hydraulic fracturing of tight shale formations. It was found that the electrostatic conjugation of ionic heads in zwitterionic surfactant and PECNP outermost layer initiates the molecular assembly and transforms the chemical environment of sulfate in the mixture and results in supercharged and stable nano-particle formation in high salinity produced water [20]. In this work, the possibility of PECNP complexation and non-ionic surfactants with hydration potential in aqueous solutions for scCO₂ foams compatible with high salinity brines used in CO₂-EOR is explored. Unlike the work reported on hydraulic fracturing applications [20], surfactant concentration is slightly below the Critical Micelle Concentration (CMC) for this EOR-compatible non-ionic surfactant. Raman spectroscopy and transmission electron microscopy (TEM) were employed to uncover the mechanism of synergistic electrostatic complexation between surfactant and PECNP in the bulk lamella mixture. Interfacial tension measurements were conducted between the PECNP and the surfactant prepared in high salinity produced water. The oil recovery of stabilized scCO₂ foam with ionic complexes were examined with foam injection through the cores resembling carbonate reservoirs. The main objective of this research is to understand the underlying mechanism of a highly stable polyelectrolyte complex nanoparticle system interacting with CO₂-brine interface during scCO₂ foam preparation and injection in underground formations using high salinity produced water.

2. MATERIALS AND METHODS

2.1. Material synthesis and preparation

Brine solutions were prepared in reverse osmosis (RO)-deionized (DI) water as a synthetic solution according to the composition of a Mississippian Limestone Play (MLP) brine from a well in Kansas. The synthetic brine composition is reported in Table 1. In order to prepare the salinity of 33,667 ppm and 67,333 ppm, the synthetic MLP brine was diluted by 6 and 3 times using RO-DI water, respectively.

Table 1. The final composition of the synthetic MLP brine.

Brine Composition	Concentration (mg/L)	Provider	CAS#
NaCl	163661.82	Fisher Chemical	7647-14-5
Na ₂ SO ₄	1224.30	Fisher Chemical	7757-82-6
KCl	714.93	AMRESCO	7447-40-7
MgCl ₂ .6H ₂ O	21759.36	Fisher Chemical	7791-18-6
CaCl ₂ .2H ₂ O	46886.13	Fisher Chemical	10035-04-8
SrCl ₂ .6H ₂ O	1535.60	Fisher Chemical	10025-70-4
Total	235782.11		

The SURFONIC N-120 used in this study belongs to the class of Nonyl phenol ethoxylates with a non-ionic nature (upon aqueous hydration) and 12 Ethylene oxide (EO) groups. Huntsman Chemicals, Woodlands, TX, USA (CAS # 9016-45-9), synthesized the surfactant for improved water compatibility in EOR. The EO group is a surface-active agent compatible with other nonionic surfactants and with ion active species [52]. The theoretical molecular weight and hydroxyl number of the surfactant are 748 and 75, respectively. The density is 1.066 g/mL at 25°C. The surfactant solution was prepared in 33,667 and 67,333 ppm salinities. The solution's CMC was obtained as 0.11 wt.% [28]. Therefore, the surfactant concentration in the solution was kept at 0.1 wt.% for all the experiments to preserve the surface activity of the surfactant and to avoid the foam film stratification [53].

Branched PEI was purchased from Sigma Aldrich, St. Louis, MO, USA (CAS# 9002-98-6) with a molecular weight of 25 kDa. The density and viscosity are 1.03 g/mL and 13,000 cP - 18,000 cP (at 50°C), respectively. The 1 wt.%. PEI solution was prepared in 33,667 and 67,333 ppm salinity brine. The pH of the PEI solutions was lowered to 8 through the addition of 5.5 mL of 12 N Hydrochloric acid (HCl) to 600 mL of the PEI solution at both salinities. Dextran sulfate sodium salt (DS) is a polyanion in powder form and was purchased from Fisher Chemical, St. Louis, MO, USA (CAS# 9011-18-1). Sulfur content and average molecular weight were 17- 20% and 500,000 g/mol, respectively [1]. The 1 wt.% DS solution was prepared in 33,667 and 67,333 ppm salinities.

To prepare the PECNP systems, different ratios of PEI:DS were mixed in 33,667 and 67,333 ppm salinities of diluted MLP brine with original 202,000 ppm salinity. The most optimized ratio of PEI: DS was selected for each salinity based on the zeta potential and particle size measurements [28]. In this study, four different PEI: DS ratios of 1, 2, 3 and 4 were initially mixed and tested. The prepared nanoparticle in the brine with up to 200,000 ppm salinity were stable in two ratios of 3:1:0.1 and 4:1:0.1 of PEI:DS:brine. The 3:1:0.1 ratio of PEI:DS:brine was selected based on particle size and zeta potential measurements and view cell experiments [28].

Subsequently, PEI-surfactant and the PECNP-surfactant solutions were prepared with different volumetric ratios of 1:9, 2:8, 3:7, 4:6 and 5:5. Two ratios of 1:9 and 2:8 were selected for 33,667 and 67,333 ppm salinities, respectively, based on our previously reported results with the view cell analysis [28]. The final surfactant concentration in the solutions was kept at 0.1 wt.% in PECNP-surfactant mixtures.

Mississippian crude oil was used for Core-Flooding experiments. The asphaltenes content for crude oil was 0.5 wt.%. The viscosity and density were measured as 3.88 cP and 0.82 g/cc, respectively, at 40°C. The Indiana limestone outcrops with the permeability of 135 mD were used for Core-Flooding experiments. The diameter and the length of the cores were 1.5 inches and 9 inches, respectively.

2.2. Raman spectroscopy

To perform Raman spectroscopy, solutions of surfactants, PECNP and mixtures of PECNP and surfactant were freeze dried and Raman spectra of lyophilized powders were obtained by LabRAM ARAMIS Raman spectrometer (LabRAM HORIBA Jobin Yvon, Edison, NJ) equipped with a HeNe laser as an excitation source ($\lambda = 633$ nm, power = 17 mW). The instrument specification includes 200 μ m confocal hole, 150 μ m wide entrance slit, 600 roovesg/mm grating, and 50X long working distance objective Olympus lens. Data acquisition was performed using dedicated software (LabSPEC 5- HORIBA Jobin Yvon). The samples were mounted in a computer-controlled stage and spectra were acquired over a range of 700-2400 cm⁻¹ with minimum 60 s exposure time and 10-time accumulation. The surfactant spectra was acquired for 1 wt% concentration in 33,667 ppm salinity brine, since lower concentrations were not resolved with the Raman instrument. The acquired spectra were processed according to a procedure introduced previously [20]. The raw data were imported into Matlab (MathWorks, Inc. Natick MA, USA), curves were smoothened (through binning adjacent data points), and fluorescence backgrounds

were removed by subtracting a fifth order polynomial fit to the original spectrum. Additionally, contributions of cosmic rays to each spectra were manually removed. The spectra of the mixtures of PECNP and surfactant were fit with average of surfactant and PECNP spectra using least-squares fitting method explained by Shafer-Peltier et al. [54]. Vectors representing each fit were created using the MATLAB polyval function and residuals for each fit were determined.

2.3. Transmission Electron Microscopy (TEM)

The procedure for TEM imaging of ionic solutions were described in [20]. A 5 µl volume of solutions of surfactant, PECNP and PECNP-surfactant mixture were placed onto a 300 mesh Lacey carbon copper grid (EMS LC 300 Cu), respectively, for 1 min and blotted twice with a filter paper. The 300 mesh copper grid with PECNP and PECNP-surfactant mixture was examined using a 200 kV FEI Tecnai F20 XT field emission transmission electron microscope at an electron acceleration voltage of 160 kV. TEM images were captured using a normative and standardized electron dose on an eucentric specimen stage and a constant defocus value from the carbon-coated surfaces. Images were randomly acquired in a size of (1024 x1024) pixel resolution at 10 different locations within the grid.

2.4. Interfacial Tension Measurements

An IFT setup made by the Core Laboratories Inc. was modified to analyze the effect of polyelectrolyte and PECNP on the interfacial properties of scCO₂ bubble in aqueous solutions according to axisymmetric drop shape analysis of pendant drop. The setup includes a chamber containing the aqueous phase solution and a tip housing the pendant bubble. A manual pump was used to inject the aqueous phase and an ISCO pump was used to inject the scCO₂ phase into the chamber. The scCO₂ bubble was formed on the tip of stainless steel capillary in high pressure chamber (~ 9.3 MPa) filled with Surfactant, PEI or PECNP-surfactant solutions while isothermal temperature of 40 °C was maintained with thermal jackets around the pipes and chamber. A high-resolution camera installed in front of the chamber recorded the shape of generated scCO₂ bubble on the needle and photos were analyzed by DROPimage software to calculate the interfacial tension between the scCO₂ and different aqueous phases. Figure 1 depicts the schematic of the employed tensiometer in this analysis. The dynamic IFT measurement was performed acquiring 1200 data points in 20 min.

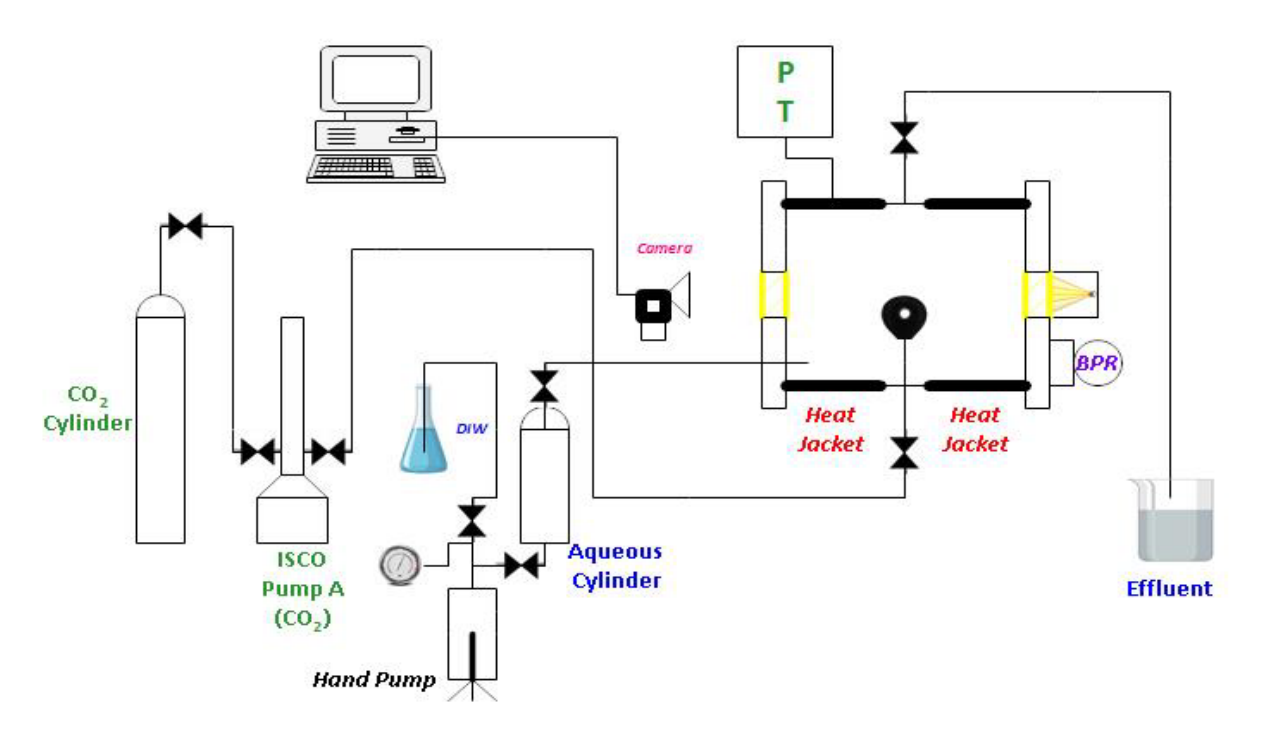


Figure 1.Schematic diagram of the high pressure-temperature interfacial tension setup, reprinted with permission from [17], Copyright SPE 2018.

2.4.1. Dilatational Elasticity

The dilatational elasticity of the surface was calculated using the data obtained from dynamic IFT measurements. Dilatational elasticity was estimated according to a ramp-type perturbation approach previously presented by Tewes and coworkers [55]. The model correlates the relative area compression to surface pressure variation over time [2]. The Tewes model was employed to measure the dilatational elasticity of the liquid film in oil-water [56,57] and scCO₂-brine [17, 20]. To describe the surface pressure change with time T, the equilibrium and non-equilibrium portions are summed up as: [55]

$$\Delta \pi = \Delta \pi_e + \Delta \pi_{ne} \tag{1}$$

Where, $\Delta \pi_e$ and $\Delta \pi_{ne}$ represent changes in surface pressure of the equilibrium and non-equilibrium parts of the curve, respectively. The equilibrium surface dilatational elasticity is expressed as: [21,55]

$$\Delta \pi_{e} = E_{e} \frac{U_{b}t}{A_{i}} \tag{2}$$

Where, A_i is the initial surface area prior to mechanical strain. The variation of interfacial pressure $(\Delta \pi_e)$ is proportional to surface area variation $(\frac{\Delta A}{A_i} = \frac{U_b t}{A_i})$ as a result of mechanical strain:

$$\Delta \pi_{e} = E_{e} \frac{\Delta A}{A_{i}} \tag{3}$$

The equilibrium surface dilatational elasticity, E_e , is calculated by measuring $\Delta \pi_e$ and calculating $\Delta A/A_i$ ratio from IFT data using Eq. (3).

Accordingly, the non-equilibrium surface dilatational elasticity, E_{ne} is determined by:

$$\Delta \pi_{ne} = \frac{E_{ne} U_b t}{A_i} \left(1 - e^{-t/\tau} \right) \tag{4}$$

Where τ stands for relaxation time. Supplementary curves for analysis are found in the SI section (Figure S1 and S2).

2.5. View Cell Durability Testing

The view cell setup was designed to withstand extreme geological conditions (T, P) and to determine the stability and durability of $scCO_2$ foam. High pressure-high temperature multifunctional foam flooding apparatus utilized with shear loop mixer, sapphire view cell, and vertical Core-Flooding (Figure 2). The foam was generated employing in-line mixing of $scCO_2$ foam (40°C, \sim 9.3 MPa) and the aqueous solution (surfactant, PEI:surfactant and PECNP:surfactant solutions) prepared in 33,667 and 67,333 ppm salinity brines with different proportions of PECNP:surfactant (1:9, 2:8). The foaming fluid was directed toward a 7 μ m Swagelok inline mixer and then to the view cell to measure the foam stability and textural properties. The effect of PEI and PECNP addition to the surfactant solution on foam generation were studied. The view cell experiments were performed to observe foam stability in the absence or in the presence of oil for foam-oil interactions. Figure 2 illustrates the schematic multifunctional foam flooding apparatus used for this study.

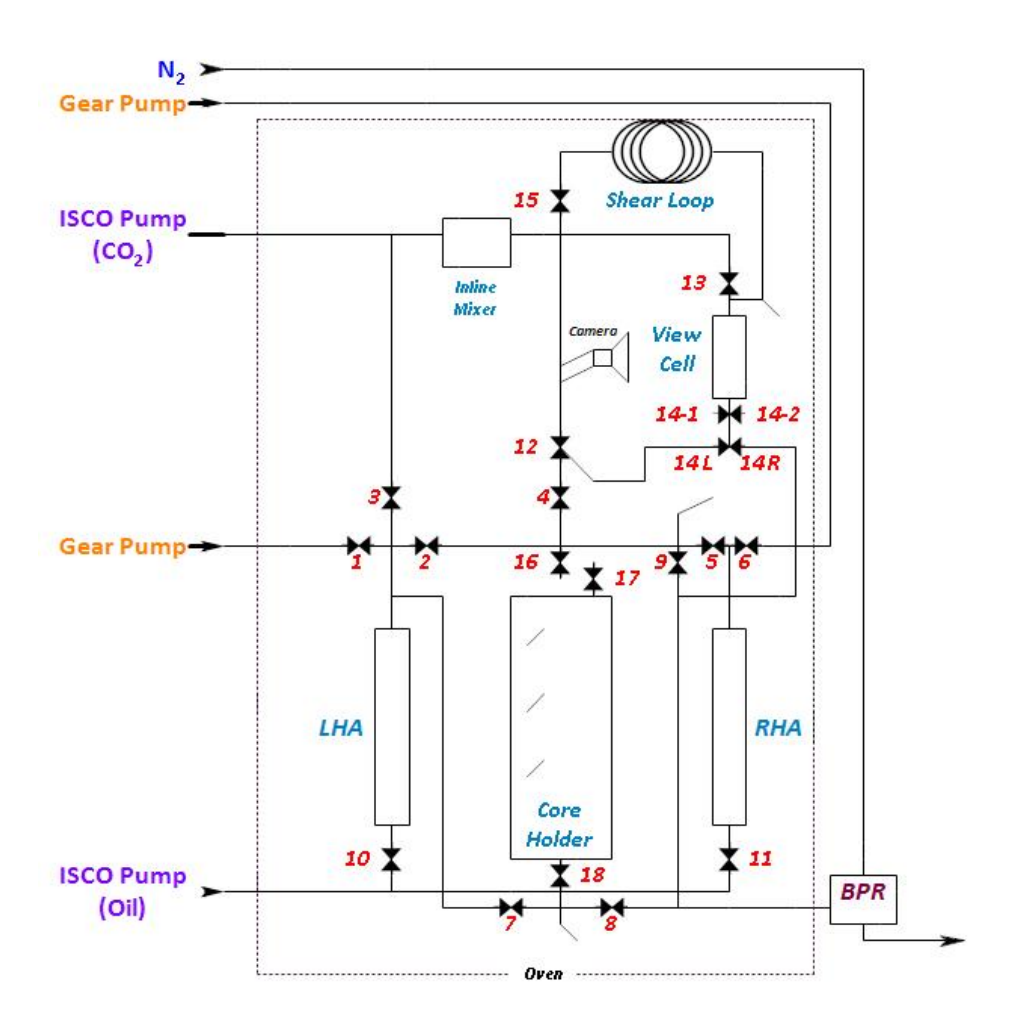


Figure 2. Schematic diagram of the Core-Flooding setup used for the view cell testing, reprinted with permission from [17], Copyright SPE 2018.

A GoPro camera was set to record the foam height on every minute and a HAYEAR camera microscope was used to observe the foam microstructure. Adobe Photoshop imaging software was employed to enhance the image quality such as light, contrast and sharpening.

2.6. Core-Flooding by CO₂ Foam

2.6.1. Porosity and Permeability Measurement

To measure permeability of core, apparent viscosity and the incremental oil recovery, Core-Flooding experiments in Indiana Limestone cores were performed. The schematic of the Core-Flooding setup is depicted in Figure 3.

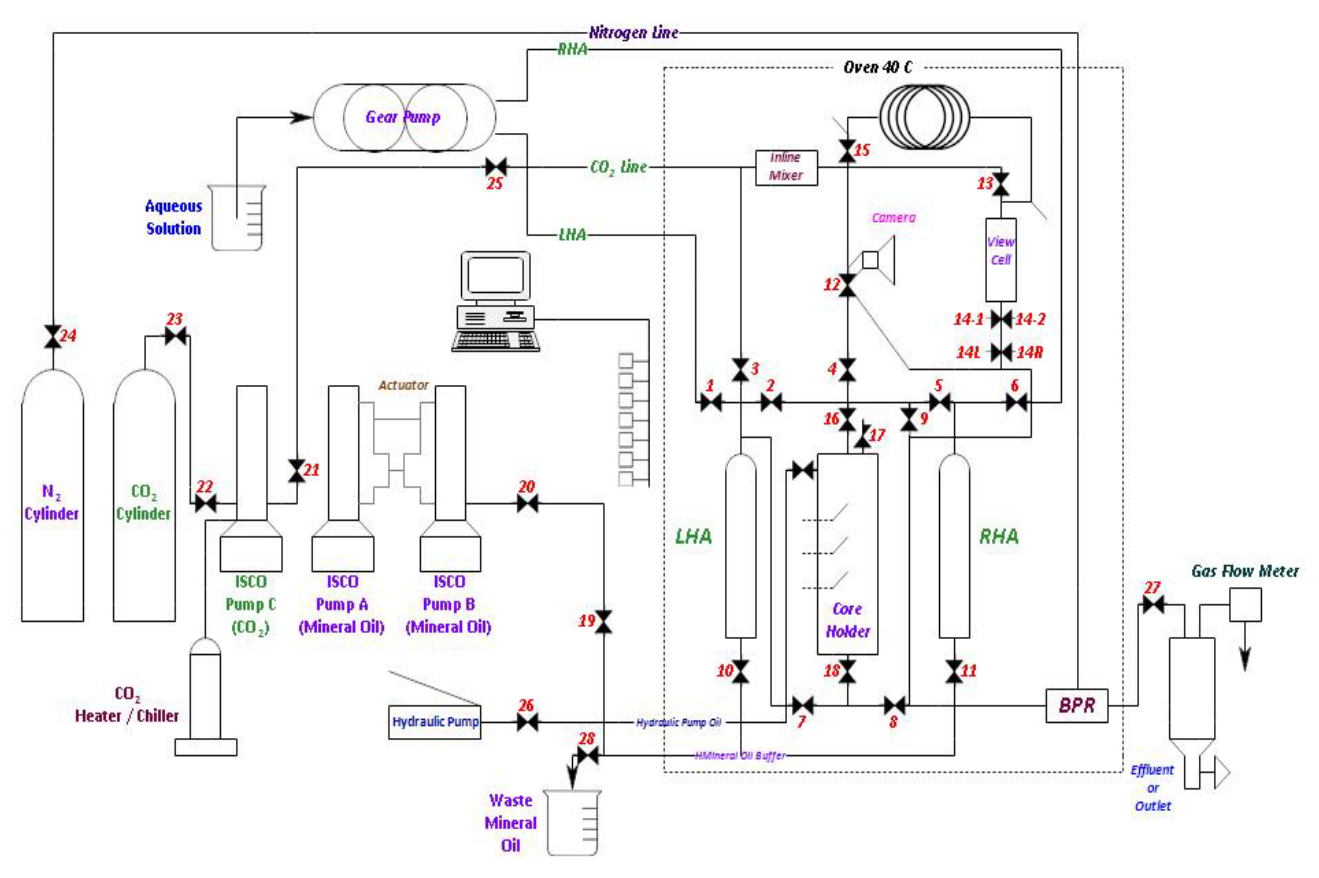


Figure 3. Schematic of the multifunctional high temperature – pressure core-flooding setup, reprinted with permission from [17], Copyright SPE 2018.

The cores were cut into the desired length of 22.86 cm and placed in the oven for 24 h at 75-80°C. The weight of the cores was measured over time until no significant weight change was observed. ~ 6.89 MPa overburden pressure was applied on the dried core and the core was vacuumed. Then, the core was saturated with the brine. The saturated weight of the core was measured to calculate the pore volume (PV) and the porosity of the core (ϕ) according to equations 5 and 6, respectively:

$$PV = \frac{\text{(Weight of the saturated core - Weight of the dry core)}}{\text{Brine Density}}$$
 (5)

Porosity
$$(\phi) = \frac{PV}{Bulk Volume (BV)}$$
 (6)

Permeability was measured for the brine saturated core. The pressure and the temperature of the setup is set to be ~ 9.3 MPa and 40°C, respectively. The brine was flowed through the core holder with different flow rates and the corresponding pressure drops were recorded. The schematic of the flow path for permeability measurement is presented in Figure 4.

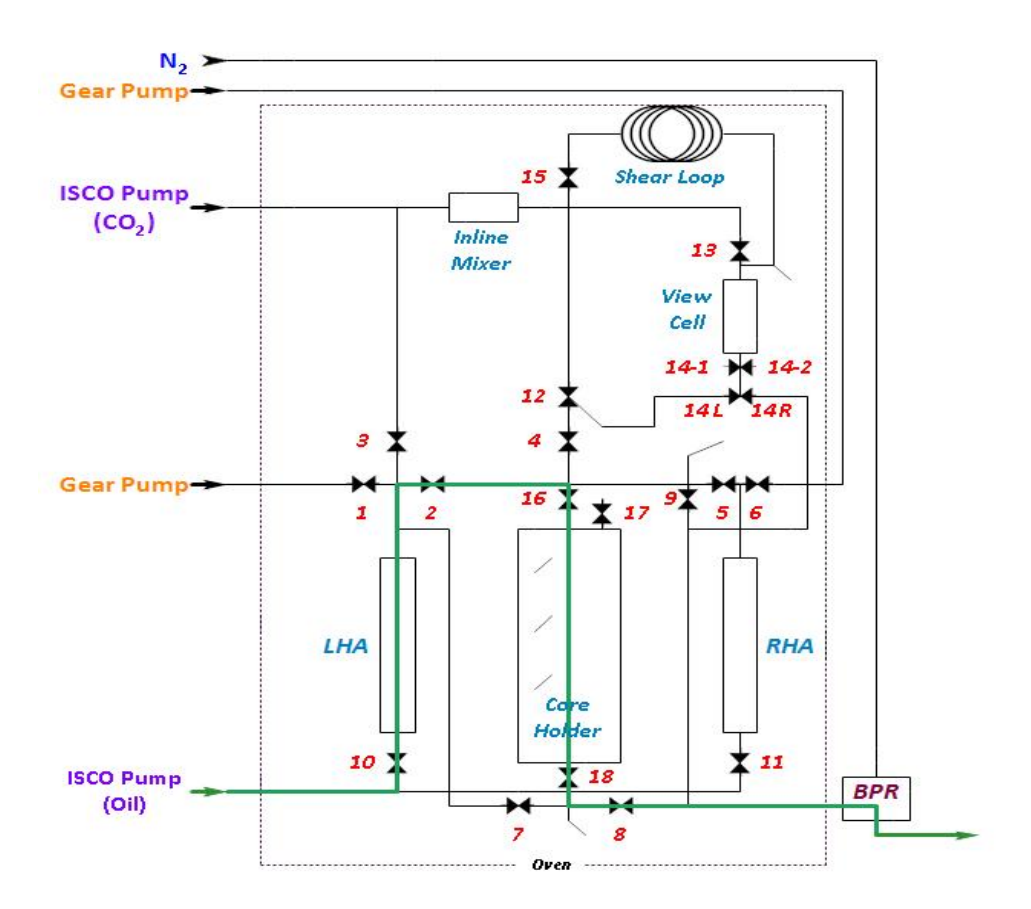


Figure 4. Schematic diagram of the flow paths to inject any aqueous phase through the core. This flow path is used during the permeability measurement, surfactant injection, PEI-surfactant injection, PECNP-injection, and water flooding, reprinted with permission from [17], Copyright SPE 2018.

The core permeability was calculated using different flow rates and pressure drops in Darcy's equation (Eq. (7)) considering the core length (L) and the viscosity of the brine (μ).

$$Q = \left(\frac{kA}{\mu L}\right) \Delta P \tag{7}$$

Where, k is the absolute permeability of the core, A is the cross-sectional area, Q is the total flowrate, and ΔP is the pressure drop along the core length [17]. The flow regime was considered laminar based on Reynolds number calculations provided in SI (Table S1).

2.6.2. ScCO₂ foam flooding in absence of crude oil in the system

To analyze the effect of PECNPs on the apparent viscosity of foaming fluid, foam flood was performed in multifunctional core flood apparatus (Figure 5). The apparent viscosity of foam was obtained by applying the steady-state pressure drops along the cores using Eq. (8) considering the properties of rocks and fluids [58].

$$\mu_{app} = \frac{kA}{q_g + q_l} \frac{|\Delta P|}{L} \tag{8}$$

where the apparent viscosity of the generated foam is shown by μ_{app} , q_g is the scCO₂ flowrate, and q_l is the flowrate of aqueous phase solution. The schematic of the flow path for the foam injection is shown in Figure 5.

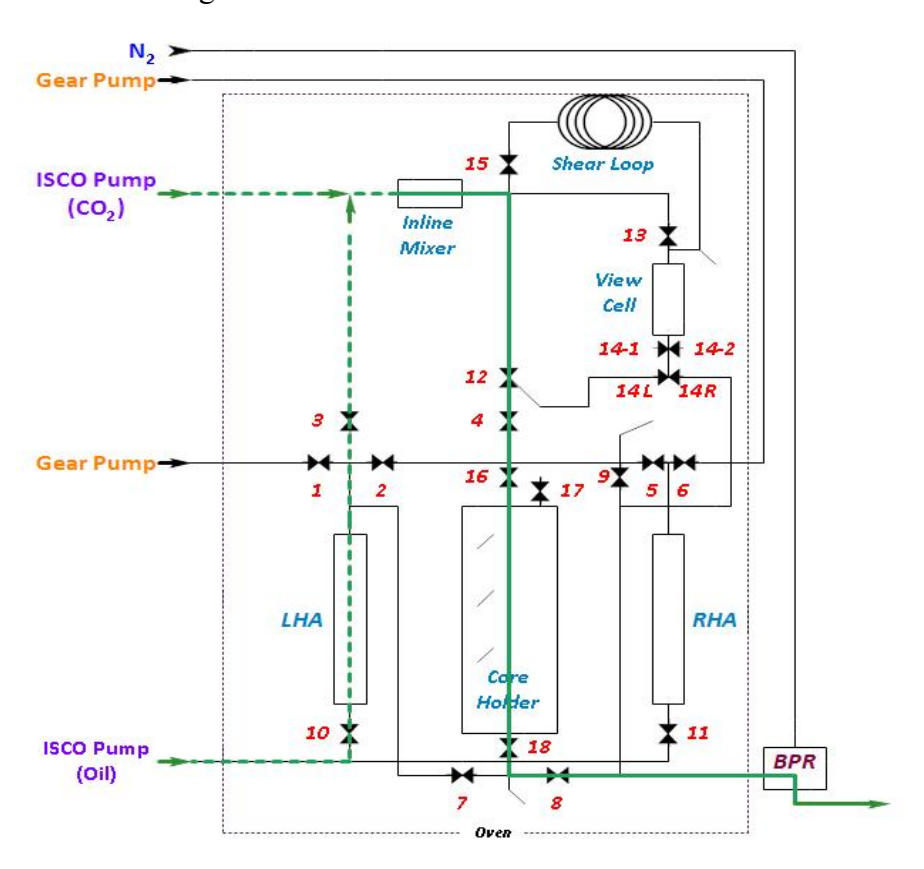


Figure 5. Schematic of the foam flow path in foam flooding through the core, reprinted with permission from [17], Copyright SPE 2018.

Subsequent to foam injection, 6 PVs of brine was injected through the core with flow rate of 3 mL/min, and the core permeability was measured to evaluate the extent of the damage to the core. Surfactant generated CO₂ foam, PEI-surfactant generated CO₂ foam, and PECNP-surfactant generated CO₂ foam were generated in two different diluted MLP brine salinities of 33,667 and 67,333 ppm and flooded into 6 different cores (#17, 13, 19, 18, 11, and 15) in the absence of crude oil.

2.6.3. Core-Flooding by scCO₂ foam in the presence of crude oil

Core-Flooding by $scCO_2$ foam in the presence of crude oil was started with primary drainage. 4 PVs of oil with the flow rate of 0.5 mL/min was injected into the core until no more water was produced. The pressure and the temperature of the system was maintained at ~ 9.3 MPa and 40°C, respectively. The volume of the collected water was recorded and used to calculate the original oil in place (OOIP) and the initial oil saturation (S_0) using equations 9 and 10:

$$OOIP = (Injected oil - produced oil)$$
 at the end of primary drainage (9)

$$S_o = \frac{00IP}{PV} \tag{10}$$

The brine was injected into the oil-saturated core with the flow rate of 0.5 mL/min, until no more oil was produced. 4 PV of brine was injected into the core. The recovery efficiency of the water flooding process, the residual oil after water flooding and the residual oil saturation (S_{or}) were calculated considering the amount of the produced oil at the end of the water flooding process using the following equations:

Waterflooding efficiency (%) =
$$(\frac{\text{Produced oil at the end of water flooding}}{\text{OOIP}}) \times 100$$
 (11)

Residual oil after water flooding = 00IP - Produced oil due to water flooding (12)

$$S_{or} = \frac{\text{(Residual oil volume after water flooding)}}{PV}$$
 (13)

Injection of the scCO₂ and the stabilizing liquids through a 7 µm inline filter results in generating the foam. The pre-generated foam with 90% quality and 3 mL/min injection rate was diverted into the core and displaced the oil in place. Surfactant generated, PEI-surfactant generated, and PECNP-surfactant generated CO₂ foams were injected through different cores with sequences described in section 3.7. Accordingly, the recovery efficiency of each flood and the residual oil saturation after the floods were calculated. At the end of each scenario, cores were flooded with up to 5 PVs of brine.

3. Results and Discussion

3.1. Transmission Electron Microscopy (TEM)

Morphological graphs of nanoparticles and surfactants in high salinity brines agree with the data obtained from previously reported light scattering results [28]. Figure 6 represents the TEM images for 0.1 wt.% surfactants, PECNP, and PECNP:surfactant (with 1:9 ratio) prepared in

33,667 ppm salinity brine. The 0.1 wt.% surfactant solution in the high salinity brine exhibits the formation of micellar domains with less than 100 nm dimensions (Figure 6a, b and c). Formation of PECNPs as soft matters made by electrostatic interaction between PEI and DS is illustrated in Figure 6d, e, and f. The electrostatic bonding between the PEI-DS complex and the surfactant is illustrated in Figure 6 g, h and i. The size range of PECNPs is consistent with the predicted values of dynamic light scattering measurements (~ 200 nm) [3].

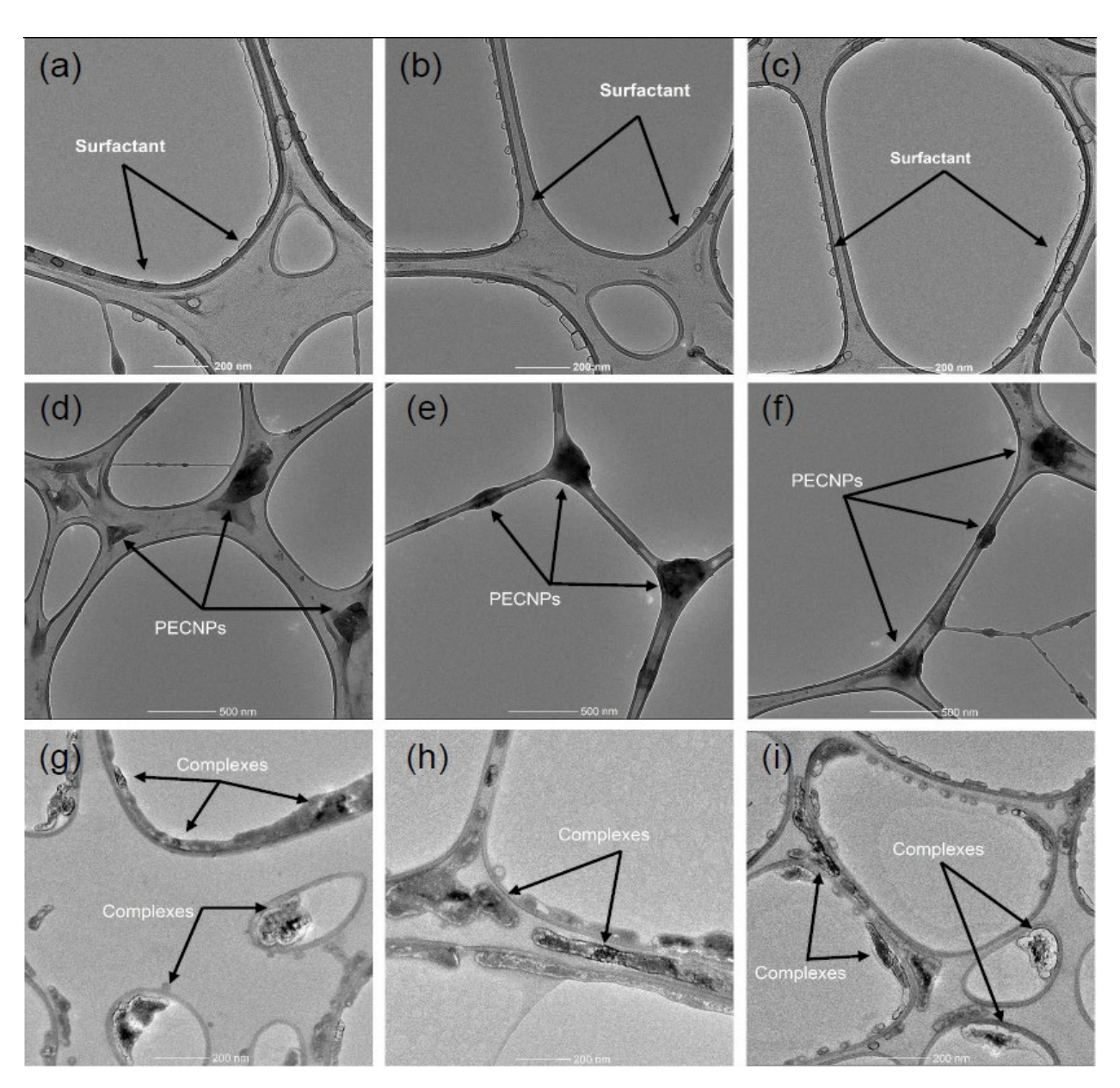


Figure 6. TEM images for 0.1 wt. % surfactant (a, b and c), PECNP (d, e and f), and complexes of PECNP: Surfactant 1:9 (g, h and i) prepared in 33,667 ppm salinity brine

Nanoparticle aggregation with N-120 micelles forms wormlike or vesicular structures comprising both nanoparticle and surfactant components electrostatically merged into each other. Figure 6 f, g, and h illustrate the complexation of PECNP and N-120 micelles. Redistribution and direct bonding of micelles on nanoparticles is due to electrostatic attractions between the amine groups in PECNP and hydrated ether and hydroxide groups in N-120. The Raman spectroscopy data supports this interpretation. Accumulation of elastic and positively charged hydrophilic particles (complexes of PECNP-surfactant) at the plateau border and lamella interface hinders liquid drainage and foam coarsening.

3.2. Raman Spectroscopy

Figure 7 shows the Raman spectra and identified characteristic bands for lyophilized samples of brine, sulfate, 1 wt.% surfactant, PECNP and PECNP-surfactant prepared in 33,667 ppm salinity brine.

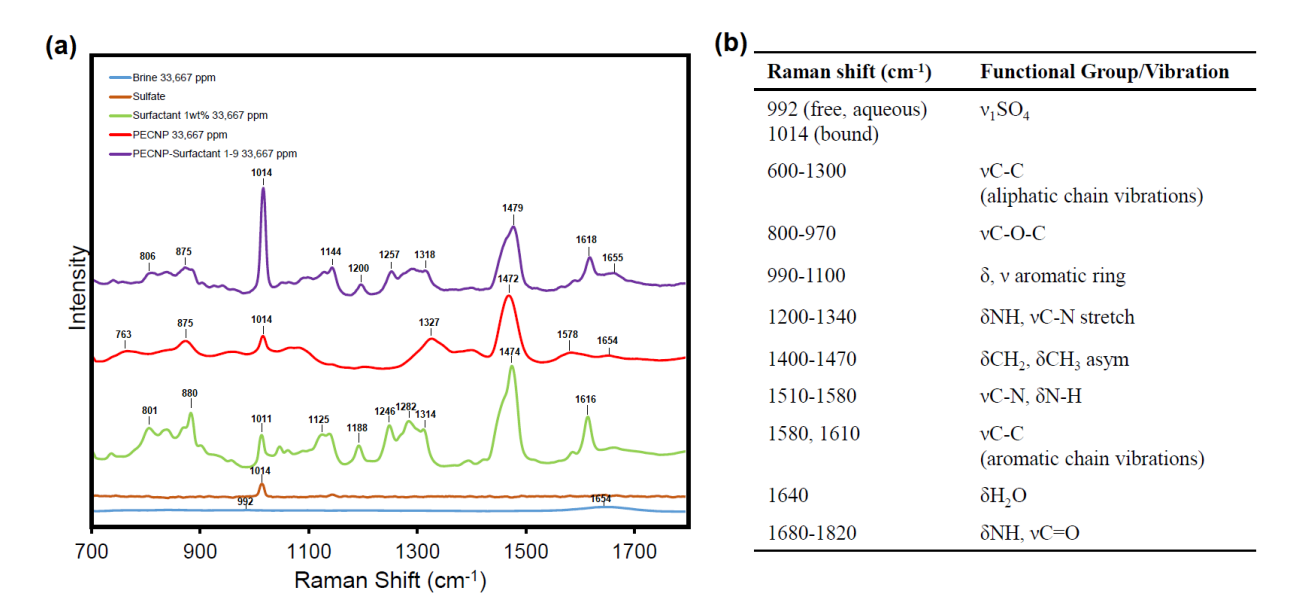


Figure 7. (a) The Raman spectra for ionic species comprising the CO₂-water lamella interface (b) Table of key Raman bands and corresponding groups based on reported values in the literature [59,60].

The strong Raman band observed at 1014 cm⁻¹ in the sulfate and PECNP spectra is characteristic of bound sulfate (Figure 7b). Its intensity varies greatly in lyophilized form, most likely due to orientation and potential concentration effects of the lyophilization process, and thus the sulfate contribution is being treated as a separate basis spectrum [20] (Figure 7a). The sulfate band overlaps with the aromatic ring vibrations present in the N-120 spectrum at 1011 cm⁻¹ and therefore the band observed at 1014 cm⁻¹ in the PECNP-surfactant spectrum is likely the result of

contributions from both sulfate and aromatic ring vibrations. Free sulfate (SO₄-2) from the Na₂SO₄ dissolved in the brine can be found at 992 cm⁻¹, in agreement with the literature [20,61]. Bands between 1011 cm⁻¹ and 1474 cm⁻¹ represent a combination of aliphatic C-C bond vibrations, aromatic ring vibrations, and anti-asymmetric -CH₂,-CH₃ vibrational modes in the surfactant backbone, while the band 1613 cm⁻¹ indicates further existence of the aromatic ring present in N-120 structure connecting the ethoxylated heads to the aliphatic tale (N-120 structure in SI). The PECNP spectrum comprises the characteristic surface functional groups including sulfate and amine. The sulfate vibrational mode from dextran sulfate is located at 1014 cm⁻¹. The relative intensity of sulfate band varies significantly among the spectra of PECNP, surfactant and the mixture of PECNP-surfactant. This observation is consistent with our previously reported results for shift and intensification of SO₄²⁻ as a result of electrostatic complexation between zwitterionic surfactant and PECNPs [20]. Bands centered at 1327 cm⁻¹ and 1578 cm⁻¹ represent the δ_{N-H} stretch and in plane bending generated by the nitrogen-hydrogen bonds as unique feature of the polyethyleneimine [20]. The wide band centered at 1654 cm⁻¹ in the brine is shared with other samples and can be attributed to the remaining water present in the lyophilized samples [20,62,63]. The PECNP-surfactant spectrum shares the features of both PECNP and surfactant solutions.

Variations in Raman scattering for the mixture of PECNP-surfactant solution in 33,667 ppm salinity brine can be predicted and modeled with least-square fitting approach [20]. A two component model comprised of an average PECNP an average surfactant spectrum was created and used to fit four spectra collected from different locations within the lyophilized samples (Figure 8). The model was used to identify regions within the spectra where the PECNP-surfactant spectrum is not completely explained by the sum of the components, indicating a change in the chemical environment of the components when mixed. The residual when mostly noise is representative of a complete fit of the model to the mixture, whereas the presence of well-defined peaks is indicative of a change in chemical environment as a result of reactions between the individual components.

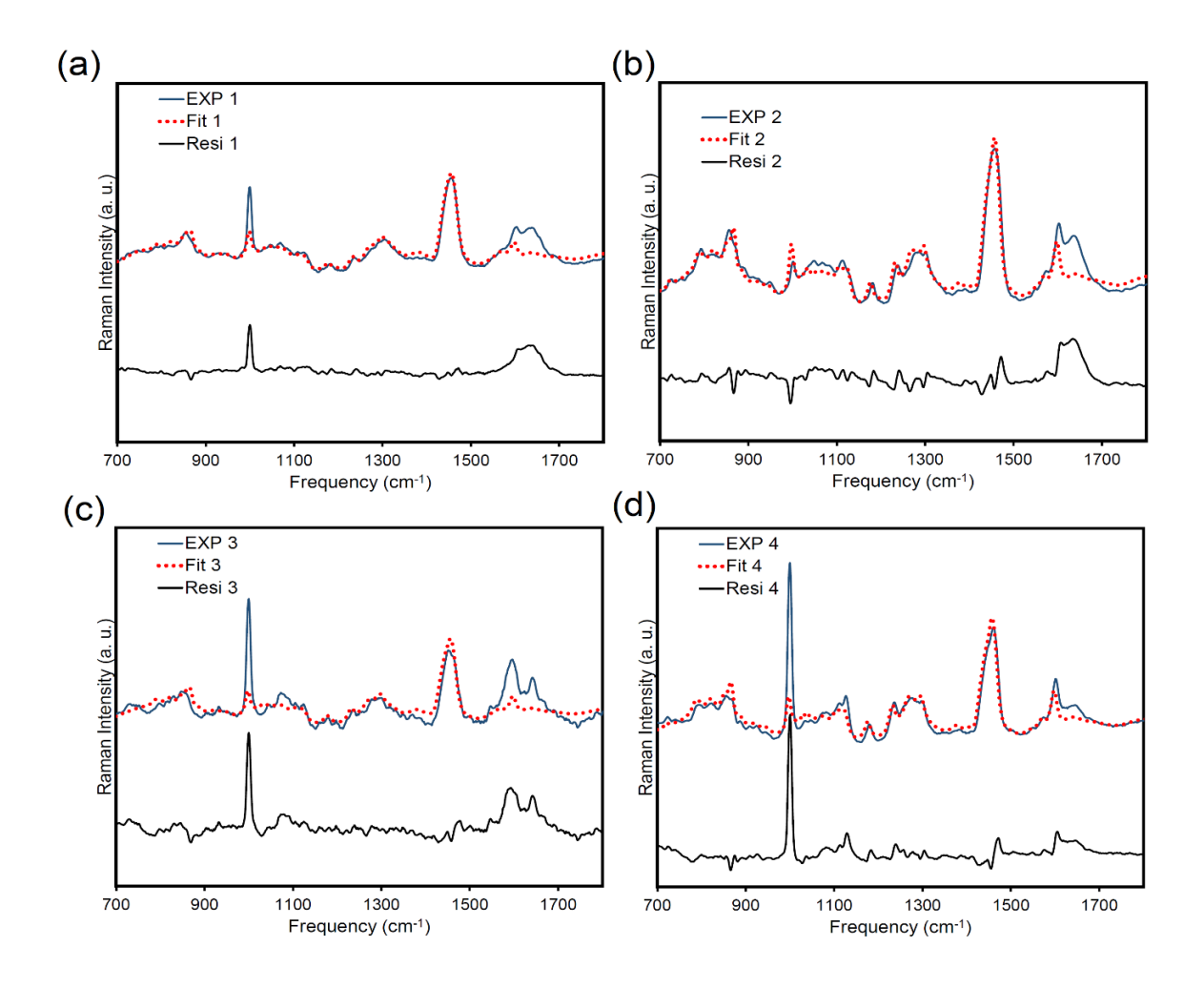


Figure 8. Raman spectra for four PECNP:surfactant (1:9 ratio) samples shown with blue line were fitted with the average spectra for PECNP and surfactant and corresponding residual line

In each residual shown in Figure 8, the sulfate band at 1014 cm⁻¹ represents a fingerprint residue and band regions between 1060 to 1100 cm⁻¹ and 1615 to 1670 cm⁻¹ are not explained with least-square model containing the features from PECNP and surfactant spectra. The sulfate intensification is due to change in chemical environment of key functional groups [20]. The residual peaks at 1060 to 1100 cm⁻¹ and between 1615 and 1670 cm⁻¹ are characteristic of aromatic and aliphatic chain vibrational modes. The strength of the intensified regions varies between samples due to inhomogeneity of the lyophilized powders.

3.4. Interfacial Tension Measurements

The CO₂ storage in geological media and deep saline aquifers is regarded to CO₂ trapping, and displacement by brine at the front of a migrating plume [64]. Critical factors in displacement such as relative permeability and capillary pressure of CO₂-brine are related to IFT of CO₂-brine

interface [64,65]. Interfacial tension (IFT) is defined as the surface tension at the interface of two immiscible fluids [28] and it controls the capillary forces within the lamellae, which is a critical property in defining the bubble rupture and drainage of foam lamella [66]. The interfacial tension between scCO₂ bubble and different systems of surfactant solution, PEI-surfactant solution, and PECNP-surfactant solution prepared in 33,667 and 67,333 ppm salinity brines were measured in dynamic mode using the pendant drop technique and results are illustrated in Figure 9a and 9b.

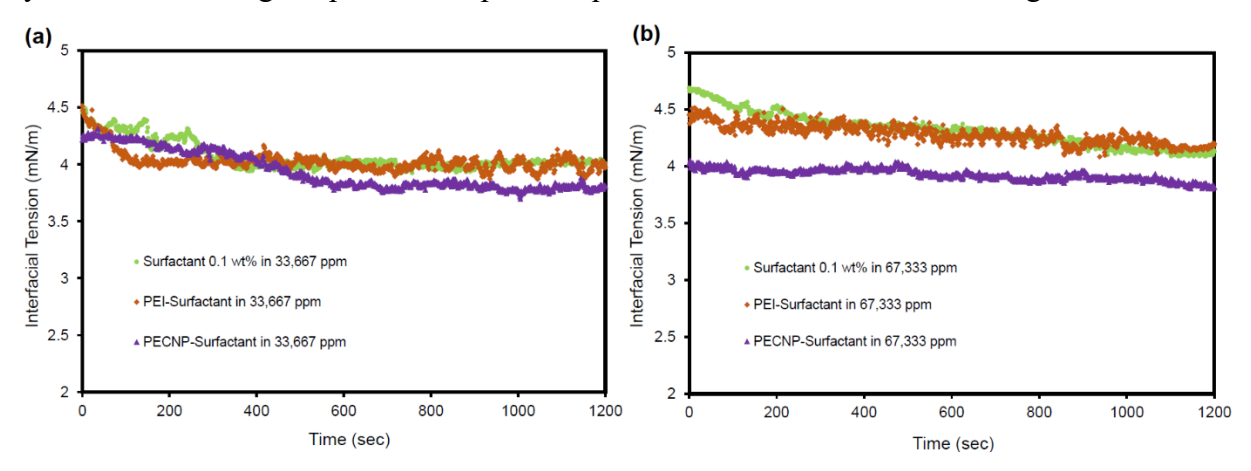


Figure 9. Comparison of the interfacial tension vs. time between a scCO₂ bubble and surfactant, PEI-surfactant, and PECNP-surfactant solutions prepared in (a) 33,667 ppm and (b) 67,333 ppm salinity of diluted MLP brine. reprinted with permission from [17], Copyright SPE 2018.

The very low IFT values of 3.79 and 3.81 mN/m were obtained (after 60 min) upon addition of 0.1 wt.% surfactant to 33,667 and 67,333 ppm salinity brines. The surfactant oligomers were able to lower the tensions and imbalanced forces at the interface and thus the capillary suction was balanced with repulsive forces of ionic complexes. The ethoxylated head groups and aliphatic-aromatic tail in N-120 demonstrate the CO₂-water compatibility. PEI addition to surfactant solution in high salinity brine fails to further reduce the tensions at the CO₂-water interface as compared to 0.1 wt.% surfactant solution. Compared to PECNP and surfactant complexes, the mixture of PEI and surfactant is not capable of forming comparably stable nanoparticles to minimize the bubble area change against the surface pressure variations mentioned by Tewes and Boury [56,67].

The results suggest that IFT declines upon addition of PECNP-surfactant complexes to the brine solution. Complexation of PECNP-surfactant forms supercharged nanoparticles reorienting from high salinity bulk phase to the interface between aqueous and scCO₂ phases, thus improving the DLVO electrostatic repulsions at the interface, which results in lamella stability. IFT reduction

results in decreasing the capillary forces and thereby lowering the mechanical energy needed to move the foam in the small pores. Literature supports the idea that IFT reduction will ultimately lead to improvements in recovery efficiency [17] and CO₂ storage capability [64]. The obtained results confirm that higher salinity results in higher IFT value for 0.1 wt. % surfactant solution due to higher presence of ionic interactions and imbalanced forces. However, formation of supercharged polyelectrolyte complexes (PECNP-surfactant) offers lower IFT in higher salinity environment (67,333 ppm) and suggests the compatibility of these nanoparticles with high concentration of ions in aqueous media, as it was previously reported that high electrolyte concentration could improve the repulsive forces and prevent the spontaneous aggregation of nanoparticles [68].

3.5. Dilatational Elasticity Measurements

To analyze the stability of the thin film liquids with surface pressure variations dilatational elasticity was calculated according to interfacial tension analysis (section 3.4). Dilatational elasticity is a measure of the surface tension gradient opposing the film drainage [21]. Figure 10 reveals the values of dilatational elasticity for scCO₂ in contact with different aqueous solutions.

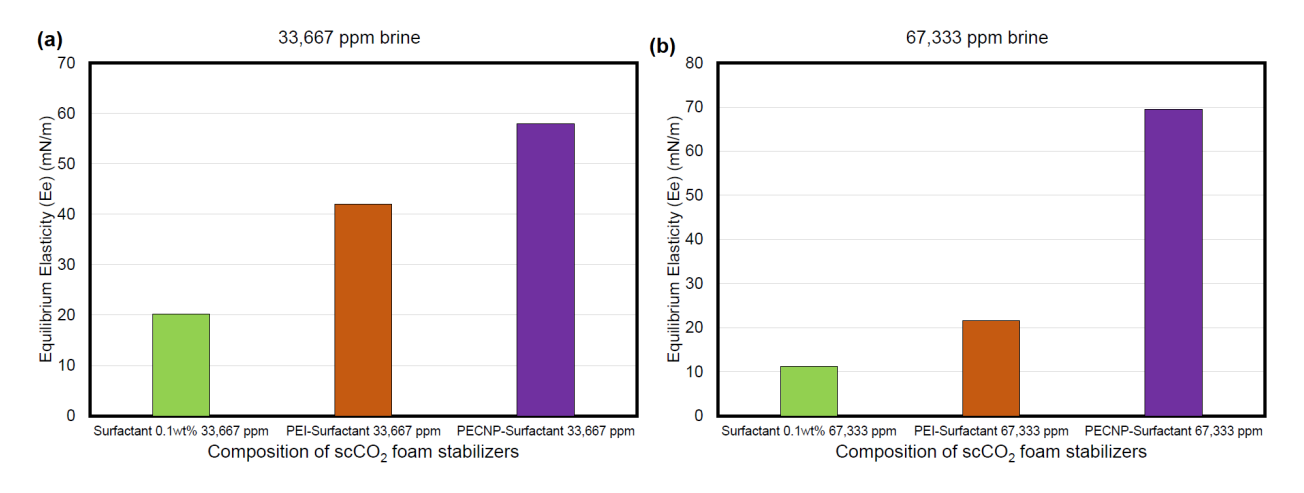


Figure 10. Equilibrium elasticity of different systems in (a) 33,667 ppm, (b) 67,333 ppm salinity of diluted MLP brine

Addition of PEI and PECNP to the surfactant solution helps to form a viscoelastic layer on the interface by accumulation of the nanoparticles on the interface [17,20]. Therefore, electrostatic complexation gives rise to the interface elasticity and mechanical strength. The formation of PECNP-surfactant agglomerates contributes to rigidity of lamella interface. Accordingly, the surface tension variation with respect to area change for PECNP-surfactant mixtures in high

salinity brine falls within the allowable range to oppose the destabilizing forces [65,67] and prolongs the bubble rupture time. Sun et. al. [70] reported that the enhanced surface dilatational viscoelasticity, maintains bubble spherical of ellipsoidal shape with prolonged time and subsequently the stability of foam is improved. The enhanced foam interfacial layer consisting PECNP-surfactant resists the deformations and shear from geological trappings, paving the way for effective CO₂ storage underground.

3.3. View Cell Durability Testing

The process of transportation and injection of CO₂/brine from industrial facilities to formation requires emulsion stability in the porous medium [71], CO₂ trapping in the liquid (solubility trapping), hydrodynamic trapping and mineral trapping [8], as stabilized lamella controls gas mobility during aquifer CO₂ storage and EOR [72]. The view cell experiments were performed to observe the durability and stability of the foam, and the foam-oil interaction. The foam height was measured with respect to time. Table 2 lists the foam lifetime in the presence and absence of crude oil for different salinities investigated in this study. The generated foams with optimum concentration of surfactant oligomers and nanoparticle (1:9 in 33,667 and 2:8 in 67,333 ppm salinity brines) remain stable for at least 60 min, due to surfactant- water solubility and PECNP compatibility to the ionic interface.

Table 2. Foam lifetime in the absence and the presence of the MLP crude oil for different CO₂ foam systems using the view cell test.

System	Decay Time (min) Without oil	Decay Time (min) with MLP crude oil		
33,667 ppm salinity of diluted MLP brine				
CO ₂ foam generated by surfactant	65	19		
CO ₂ foam generated by PEI-surfactant	115	23		
CO ₂ foam generated by PECNP-surfactant	137	36		
67,333 ppm salin	ity of diluted MLP bring	e		
CO ₂ foam generated by surfactant	50	8		
CO ₂ foam generated by PEI-surfactant	98	10		

At high electrolyte concentrations, addition of PECNP to the surfactant system significantly improves the durability of the CO₂ generated foam compared to the surfactant systems (up to 110 and 150% improvement for 33,667 and 67,333 ppm salinity brines, respectively). Foam-oil stability was also improved when the ionic complexes were formed in the lamella and foam lifetime showed up to 89 and 175% improvement for 33,667 and 67,333 ppm salinity brines, respectively. Addition of polyelectrolytes to the surfactant solution and therefore formation of supercharged positive complexes at the interface, results in increasing the disjoining pressure in the lamella opposing the drainage rate with time. The prolonged foam stability is also consistent with viscosity improvements [28] and lowering the perturbations in the interface shown with IFT results (sections 3.4, 3.5). Effect of salinity on the lifetime and durability of the foam has been extensively studied in the literature. Sedev et al. [73] reported the rise in ionic strength of solution (electrolyte concentration) to lower the thickness of the foam film according to the DLVO theory and the screening effect of the equivalent surface double layer. High salt concentration lowers the overall charge and disjoining pressure in lamellae, [73] thus facilitates the foam coalescence. Furthermore, Al-Anssari et al. [74] reported that additional surface tension caused by increasing salinity can negatively influence the stabilizing contribution of nanoparticles at the CO₂-brine interface, whereas, the PECNP-surfactant complexes used in this study successfully stabilize the interface in brines with up to 2X salinity of sea water, highlighting the necessity of electrostatic stabilization at the interface.

To analyze the effect of salinity on the generated foam and in the absence of crude oil, the 0.1 wt.% surfactant and PECNP-surfactant solutions were prepared in a 2% NaCl ppm solution as well as in diluted synthetic MLP brine solutions with, 33,667, 67,333, and 80,000 ppm total salinity. The generated scCO₂ foam systems were isolated in the view cell and the corresponding decay time was measured. Figure 11 illustrates the foam lifetime comparison between the scCO₂ foam decay time using surfactant and that of the PECNP-surfactant solutions in three different salinities. Results are consistent with recently reported data by Hosseini et. al. which demonstrated the saline resistivity of scCO₂-brine interface enhanced with electrostatic complexation of PECNP and Zwittrionic surfactants at concentrations above the CMC [20,23,26].

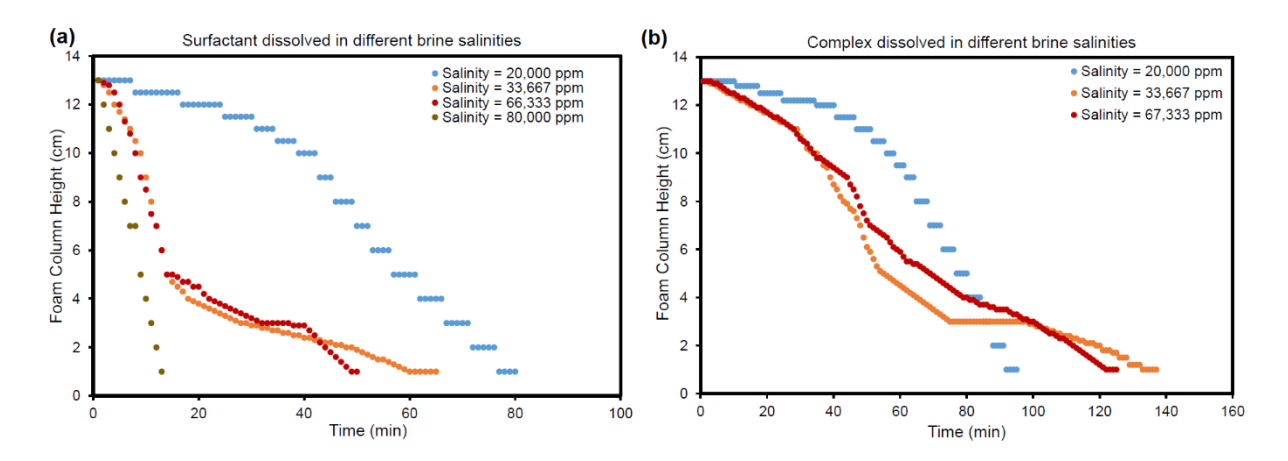


Figure 11. Comparison of the saline resistivity for (a) surfactant generated CO₂ foam and (b) PECNP-surfactant generated CO₂ foam in variety of brine salinities.

Figure 12a, b reveals the visual observation of foam column height in the isolated view cell for (a) surfactant and (b) PECNP-surfactant generated CO₂ foam in variety of salinities after 10 and 25 minutes of isolation, respectively. Formation of ionic complexes between PECNP and N-120 oligomers derives the microstructural uniformity as PECNP:surfactant with 1:9 ratio improves the bubble dispersion and hence. Figure 12c illustrates that the foam microstructure for PECNP:surfactant generated with 1:9 ratio prepared in 33,667 ppm salinity brine capable of forming microcellular gas in liquid dispersion with an average bubble diameter of approximately 200 μm. Homogenous scCO₂ bubble distribution is still preserved for stabilized foam at higher salinities compared to 2 wt.% NaCl.

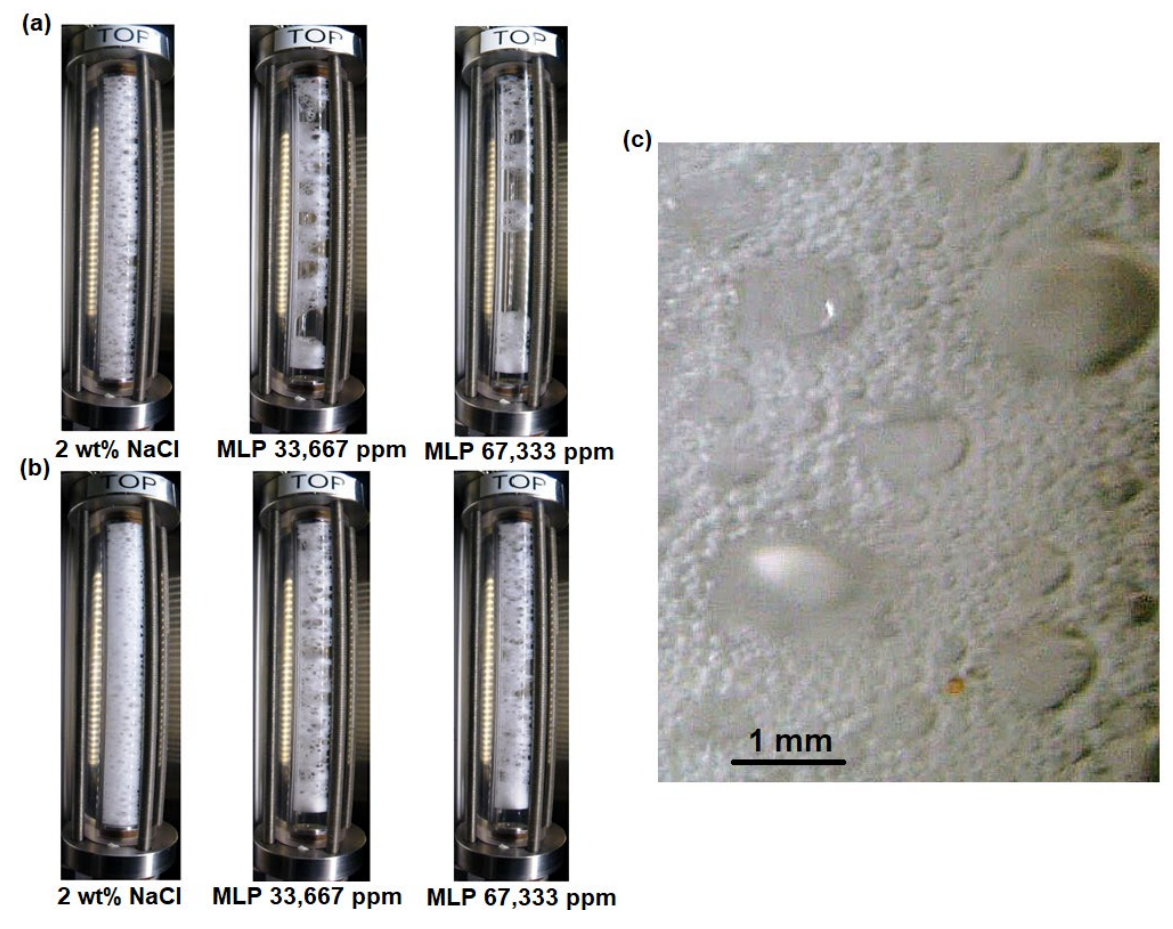


Figure 12. Foam decay in the column for (a) surfactant enhanced and (b) nanoparticle and surfactant enhanced scCO₂ foams generated in variety of salinities after 10 and 25 minutes, respectively (c) foam microstructure for PECNP-surfactant generated foam with 1:9 ratio in 33,667 ppm salinity brine

The generated foam degrades when it comes to contact with oil. The low interfacial tension between CO₂ and oil at extreme conditions triggers the oil entering and spreading in the lamella and bubble rupture [75,76]. The phenomenon is unfavorable for mobility control in oil recovery and CO₂ storage and chemical and electrochemical stabilization of interface can overcome PECNP degradations upon contact with carboxylic acid groups in MLP oil. Therefore, stable lamella is required upon introducing oil to foaming system. Supercritical CO₂ foams formed in 33,667 and 67,333 ppm salinity brines were exposed to MLP crude oil in a view cell and foam stability results are illustrated in SI (Figure S6), where the most stable foams with complexation of PECNP-surfactant (Figure 11b), are the most oil-resistive with slowest drainage ratio (Figure S6).

3.4. Porosity and Permeability Measurement

In order to measure the permeability, brine flooding is performed through the core in three different flow rates. Details of calculations are found in SI. Tables S3 and S4 represent the measured material properties and porosity and permeability of different cores used in this study. The porosity and permeability of different cores used in this study varies between 0.17 to 0.19 and 90 to 190 mD, respectively.

3.5. Foam Flooding

Primary flood was performed with two pore volumes of corresponding aqueous phase solution. Subsequently, cores were flooded with scCO₂ foam containing PECNP and surfactant stabilizing mixtures. Figure 13 illustrates the differential pressure buildup by flood of scCO₂ foam made in 33,667 and 67,333 ppm salinity brines, respectively.

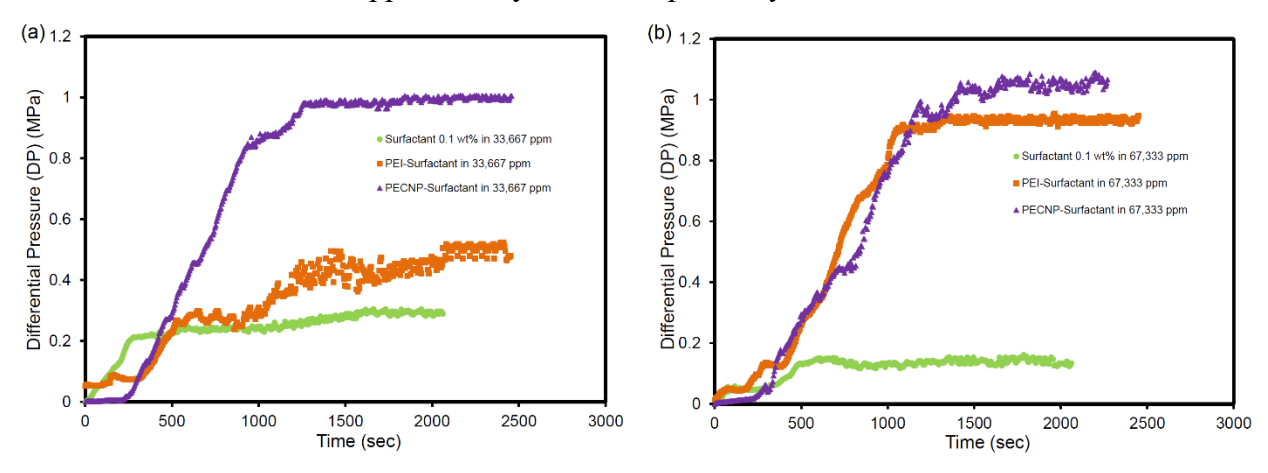


Figure 13. Differential pressure recorded for scCO₂ foam flow in carbonate rock. The liquid portion of foam is made of (a) 33,667 ppm and (b) 67,333 ppm salinity brine, reprinted with permission from [17], Copyright SPE 2018.

Resistance to flow within the core holder and the resulting differential pressure vary for different stabilizing mixtures (Figure 13). Synergistic effect of nanoparticle and chemical additives offers a noticeable differential pressure increase in 33,667 ppm salinity brine (Figure 13a). The foam flood test with PEI conjugated surfactants offered a better performance in higher electrolyte concentration compared to its performance at 33,667 ppm. However, this system still fell short of matching the performance for PECNP-surfactant generated foams (Figure 13b). PEI presented some electrostatic interaction with surfactant, but it is not preventing movement of surfactant sterically since there is no electrostatic complex formed in this system. The results are consistent with foam decay measurements (Table 2 in section 3.3) highlighting the correlation of foam stability and microstructural uniformity effect on lowering the flow resistance in porous media.

Recently, Khajehpour et. al. [77] reported similar effect in synergistic stabilization of surface treated silica nanoparticle and sulfonated surfactants for N₂-generated foams.

Table 3 lists the apparent viscosity derived from various foam floods into the Indiana Limestone cores. scCO₂ foam fluids, comprising the PEI and PECNP addition to N-120 surfactant in high salinity brine, were promising in increasing the differential pressure across the cores and so the apparent viscosity of foam improves dramatically from 3.82 to 9.19 cp in 33,667 ppm salinity and from 2.47 to 13.21 cp in 67,333 ppm salinity brine (Darcy law). Electrostatic complexation of ionic ingredients in the bulk fluid gives rise to the viscosity and bulk rheological properties and stabilizes the foam front for oil recovery [17,28]. Therefore, the miscible oil recovery and macroscopic sweep efficiency are improved due to dissolution of scCO₂ in oil and lesser portion of water (90% foam quality) used for flood [78,79].

Table 3. The apparent viscosities of the generated CO_2 foam with different aqueous phase solutions prepared in 6 and 3 times diluted MLP brine under 2000 s^{-1} shear rate.

Core #	Aqueous Phase Properties	μ _{app} (cP)
33,667 ppm salinity of diluted MLP brine		
1	Surfactant generated CO ₂ foam	3.82
2	PEI-Surfactant generated CO ₂ foam	7.94
7	PECNP-Surfactant generated CO ₂ foam	9.19
67,333 ppm salinity of diluted MLP brine		
4	Surfactant generated CO ₂ foam	2.47
8	PEI-Surfactant generated CO ₂ foam	7.10
9	PECNP-Surfactant generated CO ₂ foam	13.21

3.7. Oil recovery with different injection scenarios

Different scenarios of scCO₂ foam injections are presented in Table 4. Oil saturation and recovered oil after each flood were calculated using Equations 10 and 13.

Table 4. Different scenarios of scCO₂ foam injection in 33,667 and 67,333 ppm salinity brine. The percentages are based on the oil in place at the end of the previous flood. The values with a * signs were neglected based on the error limits. reprinted with permission from [17], Copyright SPE 2018.

First Scenario				
Salinity	33,667 ppm	33,667 ppm	67,333 ppm	67,333 ppm
Core Type	Core # 17	Core # 17	Core # 13	Core # 13
System	Oil Saturation (fraction)	Recovered Oil (%)	Oil Saturation (fraction)	Recovered Oil (%)
Primary Drainage	0.612		0.654	
Water flooding	0.284	53.58	0.350	46.60
Surfactant generated CO ₂ foam	0.155	45.33	0.220	36.96
PECNP-surfactant generated CO ₂ foam	0.140	10.00	0.196	10.75
PEI-surfactant generated CO ₂ foam	0.139*	0.80	0.188*	4.38
	Second Scena	ario		
Salinity	33,667 ppm	33,667 ppm	67,333 ppm	67,333 ppm
Core Type	Core # 19	Core # 19	Core # 18	Core # 18
C4	Oil Saturation	Recovered Oil	Oil Saturation	Recovered Oil
System	(fraction)	(%)	(fraction)	(%)
Primary Drainage	0.512		0.540	
Water flooding	0.267	47.76	0.291	46.17
PECNP-surfactant generated CO ₂ foam	0.122	54.35	0.152	47.71
PEI-surfactant generated CO ₂ foam	0.097	20.46	0.131	13.82
Surfactant generated CO ₂ foam	0.095*	2.34	0.123*	8.02
	Third Scena	rio		
Salinity	33,667 ppm	33,667 ppm	67,333 ppm	67,333 ppm
Core Type	Core # 11	Core # 11	Core # 15	Core # 15
Systems	Oil Saturation	Recovered Oil	Oil Saturation	Recovered Oil
System	(fraction)	(%)	(fraction)	(%)
Primary Drainage	0.715		0.648	
Water flooding	0.383	46.45	0.350	45.93
PEI-surfactant generated CO ₂ foam	0.259	32.45	0.213	39.20
PECNP-surfactant generated CO ₂ foam	0.236	8.58	0.192	10.08
Surfactant generated CO ₂ foam	0.221*	6.57	0.190*	1.12

Similar injection scenarios involving different foam systems in 33,667 and 67,333 ppm salinity brines were applied to core #17 and #13. Subsequent to water flood (33,667 ppm salinity

brine), 2 PV surfactant enhanced scCO₂ foam flood in core #17 resulted in recovering 45.33% of the residual oil. The foam injection was maintained until complete oil recovery was achieved. Thereafter, the core was flooded with 2.5 PV of PECNP-surfactant generated scCO₂ foam. Corresponding scCO₂ foam flood with ionic complexes enhancing the lamella produced 10.00% of the residual oil in place after surfactant-generated scCO₂ foam injection. Eventually, performing the injection of PEI-surfactant scCO₂ foam did not offer a promising oil recovery in 33,667 ppm salinity brine (0.8 %).

Similar foam injection scenario with 2X concentration of sea level water (67,333 ppm salinity) was applied to core #13 starting with water-flood and surfactant generated scCO₂ foam flood leading to production of 46.60 % of the residual oil in place. The surfactant generated scCO₂ foam injection was followed until no more oil was produced. Thereafter, 2.5 PV injection of PECNP-surfactant generated scCO₂ foam flood produced 10.75% of the residual oil in place after surfactant-generated scCO₂ foam injection. Following that, PEI-surfactant generated CO₂ foam injection through the core recovered 4.38% of the residual oil in place. Comparing the recoveries for core #17 and 13, the efficiency of foams made with lower concentration of brine to recover more oil is evident. However, presence of PEI-surfactant in scCO₂ foam demonstrates significant gain in production in the last step of flooding scenario in 2X concentration of sea level brine.

A different sequence of scCO₂ injection listed in Table 4 was tested in 33,667 and 67,333 ppm salinities of diluted MLP brine for core #19 and #18. The cores were flooded with brine and PECNP-surfactant generated scCO₂ foam. Injections led to 54.35% and 47.71% recovery of the residual oil in place for cores #19 and #18, respectively (compared to 45.33, 36.96 % in the first scenario). More stable foam leads to up to 22% increase in oil recovery in the first step after water flood. Subsequently, 2.5 PVs of PEI-surfactant generated CO₂ foam recovered 20.46% of the residual oil in place for core #19 and 13.82% of the residual oil in place for core #18. Finally, 2.5 PVs of the surfactant enhanced CO₂ foam recovered 2.34% of the residual oil in place for core #19 and 8.02% of the residual oil in place for core #18. The second scenario was clearly more successful in decreasing the residual oil saturation and improving oil recovery, mainly due to advanced scCO₂ flood with supercharged complexes forming the lamella where the most of oil trapped in porous media was displaced by stabilized foam front.

Eventually, in the last scenario, core #11 and core #15 were subjected to the last sequence of injection between PEI, surfactant and complex enhanced scCO₂ foams. Initially, the core was

flooded with the PEI-surfactant generated scCO₂ foam. Injection of the 2.5 PV of PEI-surfactant generated scCO₂ foam led to 32.45% and 39.20% recovery of the residual oil in core #11 and core #15, respectively, and it was maintained until complete production was achieved. Subsequently, injection of 2.5 PVs of PECNP-surfactant generated scCO₂ foam recovered 8.58% of the residual oil in the core #11 and 10.08% of the residual oil in core #15. Finally, 2.5 PVs injection of surfactant generated CO₂ foam through the cores recovered 6.57% of the residual oil in core #11 and 1.12% of the residual oil in core #15. Figure 14 reveals the total recovered oil in different scenarios for variety of cores according to the order of injections.

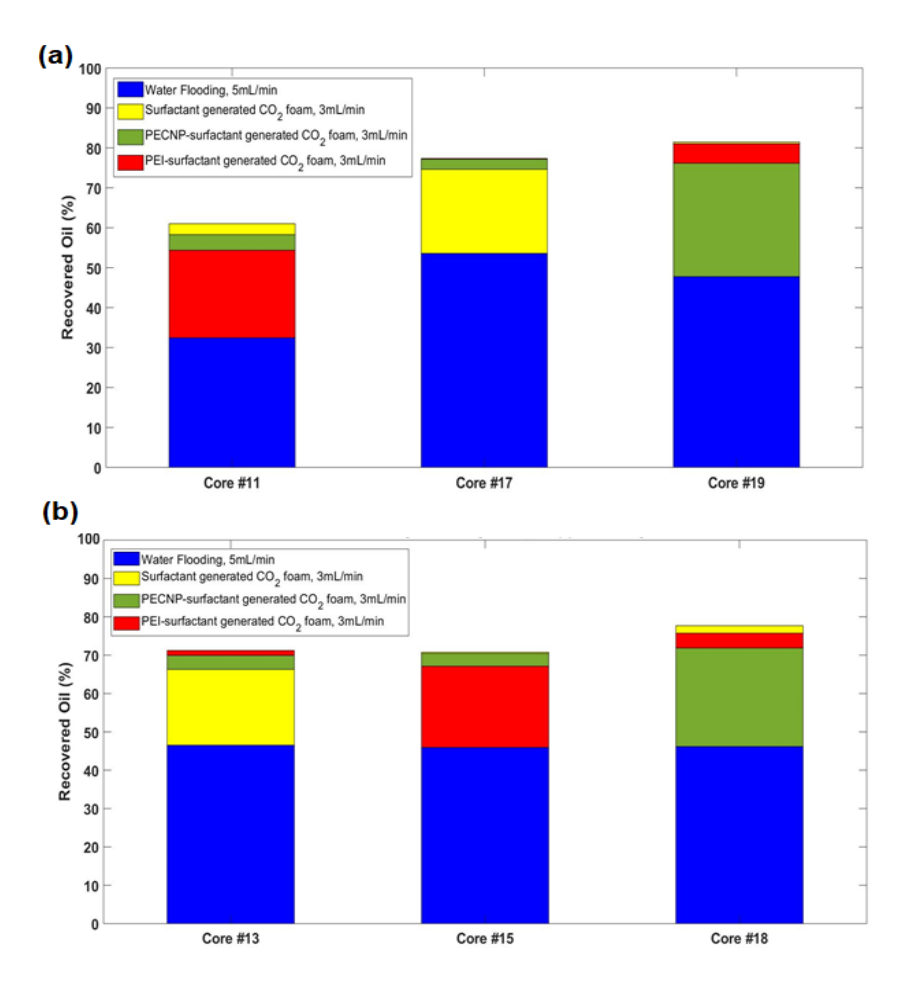


Figure 14. The summary of recovery factors for different injection in (a) 33,667 ppm (b) 67,333 ppm salinity of diluted MLP brine. The order of the injection are shown from the bottom to the top of each bar.

The recovery factor and the residual oil saturation values listed in Table 4 exhibit that the second scenario leads to the highest oil production and the highest values of recovery factor for both 33,667 and 67,333 ppm salinities of diluted MLP brine. In general, the first scenario is considered for the oil wells subjected to surfactant foam flooding and thus are at the residual oil

saturation condition. Injection of the PECNP-surfactant generated scCO₂ foam after surfactant foam flooding recovered 10% of the residual oil in place due to improved stability of the PCNP-generated scCO₂ foams in the presence of crude oil. Electrostatic hindrance of the polyelectrolyte complex nanoparticles to the N-120 surfactants stabilizes the interface by preventing the surfactants from leaving the interface. Therefore, generated foams are stabilized in the presence of crude oil in high salinity environment. PEI adds to charge density and stability of the interface as well. However, the charge density and colloidal stability is not enough to compete with repulsion forces offered by PECNP-surfactant complexes. The stability of generated foams is coupled with the improvement effect of PECNPs on viscosity of the aqueous phase (rheological data are found in SI).

4. Conclusions

Herein, we reported the improved capability of dry scCO₂ foams stabilized with polyelectrolyte complex nanoparticles (PECNP) for Enhanced Oil Recovery (EOR) applications, storage and sequestration. The internal phase emulsion stabilized with PECNP combines the improved viscosity and stability to flow in geological formations and sweep the oil in porous media. A novel mixture containing N-120 surfactant and PECNP is effective in immobilization of lamella, rigidity improvement and electrostatic repulsion in CO₂-water interface to improve the recovery and reservoir depletion while the gas phase is stored partially. The major conclusions are summarized as following:

- 1. The presented mixture offers the potential to reduce produced water disposal and fresh water usage for EOR in conventional oil reservoirs. The chemical compatibility of scCO₂ with produced water (with up to 67,333 ppm salinity) introduces a viable solution for sustainability of water-based energy production and environmentally friendly approach to manage the water resources on the ground and greenhouse gas control in the atmosphere.
- 2. A novel ionic complex containing PECNP and N-120 ethoxylated surfactant is capable of enhancing interfacial interactions and disjoining pressure of the thin film of high salinity brine formed between scCO₂ bubbles and can act as improved DLVO forces in aqueous polyelectrolytes for carbonate surfaces. TEM imaging and Raman spectroscopy analysis confirm the PECNP's electrosteric interaction with N-120 micelles as wormlike or vesicular structures comprising both nanoparticle and surfactant components. The ionic nano-structures offer noticeable IFT reduction

and also provides improvements in rigidity of lamella against the surface tension variations at the interface, opposing the lamella drainage and bubble coalescence.

- 3. Raman spectroscopy results were used to understand the chemical interaction between N-120 oligomers and the PECNPs. A two component model comprising an average PECNP and an average surfactant was fit to Raman spectra of lyophilized PECNP:surfactant solution with 1:9 ratio. The model enabled identification of three major spectral regions not explained by the N-120 and PECNP spectra alone, indicating a change in chemical environment of the key functional groups as a result of ionic complexation and reorganization of the aromatic and aliphatic chain components.
- 4. A comparative study of scCO₂ foam generation with variety of ionic stabilizers at the interface demonstrated the superior capability of PECNP-surfactant conjugation in homogenous microcellular foam formation with lowering the IFT, improving the dilatational elasticity and mechanical strength at the interface. Therefore, foam stability and lifetime is drastically increased, compared to surfactant and PEI-surfactant solutions forming the lamella. The supercharged complex generated a longer lasting foam in the presence and absence of crude oil. Since the mixture is chemically compatible with electrolyte concentration up to 67,333 ppm salinity (2X concentration of seawater), PECNP-surfactant mixtures represent a new prospect for stabilizing the thin films in a high salinity environment.
- 5. Addition of PEI and PECNP to N-120 surfactant improved the foam sweep efficiency and oil recovery from carbonate reservoirs employing high concentration of brine electrolytes. Highest pressure drop along the core was observed for PECNP-surfactant generated scCO₂ foam, which corresponds to the highest average effective viscosity for stabilizing electrolyte. Variety of scenarios of foam injection tested on oil saturated carbonate core samples indicated the highest incremental oil recovery and lowest oil saturation are achieved by prioritizing PECNP-surfactant scCO₂ foam flood in both electrolyte concentrations. Injecting the PECNP- surfactant generated CO₂ foam after the injection of surfactant foam and reaching the residual oil state is recommended since this injection sequence recovered 10% of the residual oil in place.

Acknowledgements

Authors would like to thank the National Science Foundation EPSCoR Research Infrastructure Improvement Program: Track -2 Focused EPSCoR Collaboration award (OIA-

1632892) for their partial financial support of this project. In addition, authors extend their appreciation to the Kansas Interdisciplinary Carbonates Consortium (KICC) for partially funding the project. We would also like to thank Huntsman Chemicals Inc. for providing the surfactant. The technical support from Mr. Zach Kessler from the Chemical and Petroleum Engineering department and Mr. Scott Ramskill from the Tertiary Oil Recovery Program (TORP) at the University of Kansas for installment and maintenance of the lab equipment are greatly appreciated. Authors also extend their acknowledgement to Dr. Cory J, Berkland, Matthew Christopher and Stephanie Johnson in the Pharmaceutical Chemistry Department at University of Kansas (KU) for their generous help, time and effort in freeze drying of samples and the Institute for Bioengineering Research (IBER) for access to their Raman spectroscopic system. Last but not least, the authors gratefully acknowledge Dr. Prem S. Thapa from KU Microscopy and Analytical Imaging Laboratory for the help with Transmission Electron Microscopy analysis.

ASSOCIATED CONTENT

Supporting Information (SI) is provided by the authors. A brief explanation of experimental procedures, process flow diagrams, supplementary physical property measurement for PECNP and PECNP/Surfactant mixtures, additional dilatational elasticity, foam stability, rheological data and core flood calculations are presented in SI.

AUTHOR INFORMATION

Corresponding author

*Reza Barati Ghahfarokhi, Department of Chemical and Petroleum Engineering, The University of Kansas, Lawrence, Kansas 66045, E-mail: reza.barati@ku.edu

Phone Number: (785)864-1232

Author Contribution

The manuscript was written through contributions of all authors. All authors have given approval to the final version of the manuscript.

Abbreviations

scCO₂, supercritical CO₂; CCUS, carbon capture utilization and storage; PEI, polyethylenimine; DS, dextran sulfate; PECNP, polyelectrolyte complex nanoparticle; MLP, Mississippian limestone play; RO-DI water, reverse osmosis- deionized water; CMC, critical

micelle concentration; MMP, minimum miscibility pressure; TEM, transmission electron microscopy; IFT, interfacial tension; TDS, total dissolved solids.

REFERENCES

- [1] Rogelj J, Elzen M.D., Höhne N, Fransen T, Fekete H, Winkler H, et al. Paris Agreement climate proposals need a boost to keep warming well below 2°C. Nature 2016;534:631–639.doi:10.1038/nature18307.
- [2] Luderer G., Vrontisi Z., Bertram C., Edelenbosch O.Y., Pietzcker RC, Rogelj J, et al. Residual fossil CO₂ emissions in 1.5 2°C pathways. NATURE CLIMATE CHANGE, 2018;8:626-633.
- [3] Roser M., Ritchie H., Fossil Fuels. ourworldindata.org. accessed on 07/30/2019.
- [4] Michael K., Golab A., Shulakova V., Ennis-king J., Allinson G., Sharma S., et al. International Journal of Greenhouse Gas Control, Geological storage of CO₂ in saline aquifers—A review of the experience from existing storage operations. Int J Greenhouse Gas Control, 2010;4:659–667. doi:10.1016/j.ijggc.2009.12.011.
- [5] Steeneveldt R., Berger B., Torp T.A. CO₂ capture and storage closing the knowing–doing gap, 2006;84(A9):739-763.
- [6] Hosseini, H., Thakkar, H., Krishnamurthy, A., Brennan, P. J. Rezaei, F., Rownaghi A.A. Immobilizing Metal Organic Frameworks on Active Substrates for CO₂ Adsorption, 2016 AIChE Annu. Meet., San Francisco, CA.
- [7] Nguyen D.N., Allinson W.G. The Economics of CO₂ Capture and Geological Storage, SPE 77810. 2002:8–10.
- [8] Eke P.E., Naylor M., Haszeldine S., Curtis A., CO₂ / Brine Surface Dissolution and Injection: CO₂ Storage Enhancement, SPE 124711, 2009.
- [9] Jiang L., Yu M., Liu Y., Yang M., Zhang Y., Xue Z., et al. Behavior of CO₂/water flow in porous media for CO₂ geological storage. Magn Reson Imaging. 2017;37:100–106. doi:10.1016/j.mri.2016.11.002.
- [10] Ferguson R.C., Kuuskraa V.A., Leeuwen T.S. Van. Storing CO₂ With Next Generation CO₂ -EOR Technology, SPE 139717, 2010.
- [11] Núñez-López V., Gil-egui R., Hosseini S.A. Environmental and Operational Performance of CO₂ EOR as a CCUS Technology: A Cranfield Example with Dynamic LCA Considerations, 2019.
- [12] Rognmo A.U., Fredriksen S.B., Alcorn Z.P., Sharma M. Pore-to-Core EOR Upscaling for CO₂-Foam for CCUS, SPE-190869, 2018.
- [13] DOE, Enhanced Oil Recovery, https://www.energy.gov/fe/science-innovation/oil-gas-research/enhanced-oil-recovery. Date accessed 07/30/2019.

- [14] Langston M.V., Hoadley S.F., Young D.N. Definitive CO₂ Flooding Response in the SACROC Unit. SPE/DOE 17321. 1988: 27-34.
- [15] Orr Jr F.M. Theory of Gas Injection Processes. Tie Line Publications. Stanford. 2007.
- [16] Green D., Willhite P. Enhanced Oil Recovery. Society of Petroleum Engineers. Richardson, Texas 1998.
- [17] Nazari N., Tsau J., Barati R. Improving CO₂ Foam for EOR Applications Using Polyelectrolyte Complex Nanoparticles Tolerant of High Salinity Produced Water Introduction Materials, SPE-190179, 2018.
- [18] Bernard G.G., Holm L.R.W, Lake C. Method for Recovering Oil From Subterranean Formations. United States Patent Office. 3,342,256. 1967.
- [19] Rochelle C.A., Moore Y.A. The solubility of supercritical CO₂ into pure water and synthetic Utsira porewater. British Geolological Survey Commissioned Report CR/02/052, 2002.
- [20] Hosseini H., Tsau J.S., Shafer-peltier K., Marshall C., Ye Q., Ghahfarokhi R.B. Experimental and Mechanistic Study of Stabilized Dry CO₂ Foam Using Polyelectrolyte Complex Nanoparticles Compatible with Produced Water To Improve Hydraulic Fracturing Performance, 2019;58:9431– 9449.
- [21] Schramm L.L. Foams: Fundamentals and Applications in the Petroleum Industry. American Chemical Society; 1994.
- [22] Enick R.M., Olsen D.K., Ammer, J., Schuller, W. Mobility and Conformance Control for Carbon Dioxide Enhanced Oil Recovery (CO₂-EOR) via Thickeners, Foams, and Gels A Literature Review of 40 Years of Research. SPE 154122, 2012.
- [23] Hosseini H., Tsau J., Barati R. Lowering Fresh Water Usage in Hydraulic Fracturing by Stabilizing scCO₂ Foam with Polyelectrolyte Complex Nanoparticles Prepared in High Salinity Produced Water, SPE-189555. 2018.
- [24] Xing D., Wei B., McLendon W.J., Enick R.M., McNulty S., Trickett K., et al. CO₂-Soluble, Nonionic, Water-Soluble Surfactants That Stabilize CO₂-in-Brine Foams. SPE J 2012;17:1172–85.
- [25] Al-muntasheri G.A., Houston C., Aramco S. A Critical Review of Hydraulic-Fracturing Fluids for Moderate- to Ultralow- Permeability Formations Over the Last Decade, SPE-169552. 2014:243– 260.
- [26] Hosseini H., Tsau J.S., Peltier E., Barati R. Highly stable scCO₂-high salinity brine interface for waterless fracturing using polyelectrolyte complex nanoparticles. Abstr. Pap. Am. Chem. Soc. 2018, 256, Boston, MA: ACS; 2018.
- [27] Yu J., An C., Mo D., Liu, N., Lee, R. Foam Mobility Control for Nanoparticle-Stabilized CO₂ Foam. SPE 153336, 2012:1–13.

- [28] Nazari N., Tsau J.S., Barati R. CO₂ Foam Stability Improvement Using Polyelectrolyte Complex Nanoparticles Prepared in Produced Water. Energies 2017;10:516.
- [29] Evans P., Robinson K., Limited O.P. Produced Water Management Reservoir and Facilities Engineering Aspects, SPE 53254, 1999.
- [30] Patel C., Barrufet M.A. Effective Resource Management of Produced Water in Oil & Gas Operations 2004:1–13.
- [31] Nazari N., Barati R., Tsau J.S., Peltier E. CO₂ foam: Stability improving in high salinity produced water. Abstr. Pap. Am. Chem. Soc. 2017, 254, 2017.
- [32] Caudle D.D., Produced Water Regulations in the United States: Then, Now and in the Future, SPE 77389, 2002.
- [33] Middleton R.S., Carey J.W., Currier R.P., Hyman J.D., Kang Q., Karra S., et al. Shale gas and non-aqueous fracturing fluids: Opportunities and challenges for supercritical CO₂. Appl Energy. 2015;147:500–509.
- [34] Guo H., Kovscek A.R. Investigation of the effects of ions on short-range non-DLVO forces at the calcite/brine interface and implications for low salinity oil-recovery processes. Journal of Colloid and Interface Science. J Colloid Interface Sci. 2019;552:295–311.
- [35] Yin G., Grigg R.B., Svec Y., Oil Recovery and Surfactant Adsorption During CO₂-Foam Flooding. OTC 19787. 2009.
- [36] Gland N., Chevallier E., Cuenca A., Batot G. New Development of Cationic Surfactant Formulations for Foam Assisted CO₂-EOR in Carbonates Formations, SPE-193201. 2018.
- [37] Le V.Q., Nguyen Q.P., Sanders A.W. A Novel Foam Concept with CO₂ Dissolved Surfactants. SPE/DOE Improv Oil Recover Symp. 2008.
- [38] Sagir M., Tan I.M., Mushtaq M., Pervaiz M., Suleman Tahir M., Khurram S. CO₂ mobility control using CO₂ philic surfactant for enhanced oil recovery. J Pet Explor Prod Technol. 2016;6:401–407.
- [39] Mclendon W.J., Rua N., Koronaios P., Mcnulty S., Enick R.M., Biesmans G., Miller A., Salazar L., Soong Y., Romanov V., Crandall D. Assessment of CO₂ -Soluble Surfactants for Mobility Reduction using Mobility Measurements and CT Imaging. SPE Improved Oil Recovery Symposium. 2012.
- [40] Mclendon W.J., Koronaios P., Enick R.M., Biesmans G., Salazar L., Miller A. Assessment of CO₂ -soluble non-ionic surfactants for mobility reduction using mobility measurements and CT imaging. J Pet Sci Eng. 2014;119:196–209.
- [41] Hirasaki G.J., Miller C.A., Puerto M. Recent Advances in Surfactant EOR. SPE Journal. 2011;16:889-907.

- [42] Wang, J., Han, M., Fuseni, A.B., Cao, D. Surfactant Adsorption in Surfactant-Polymer Flooding for Carbonate. SPE Middle East Oil & Gas Show and Conference. 2015.
- [43] Kristen-hochrein N., Laschewsky A., Miller R., Von Klitzing R. Stability of Foam Films of Oppositely Charged Polyelectrolyte/Surfactant Mixtures: Effect of Isoelectric Point, ACS Physical Chemistry B. 2011;115:14475–14483.
- [44] Kristen N., Von Klitzing R. Effect of polyelectrolyte/surfactant combinations on the stability of foam films. Soft Matter. 2010;6:849–861.
- [45] Barati R., Johnson S.J., Mccool S., Green D.W., Willhite G.P., Liang J.T. Polyelectrolyte Complex Nanoparticles for Protection and Delayed Release of Enzymes in Alkaline pH and at Elevated Temperature During Hydraulic Fracturing of Oil Wells. Journal of Applied Polymer Science.2012;126:587-592
- [46] Barati R., Johnson S.J., McCool S., Green D.W., Willhite P. G., Liang J.T. Fracturing fluid cleanup by controlled release of enzymes from polyelectrolyte complex nanoparticles. J Appl Polym Sci 2011;121:1292–1298.
- [47] Ghahfarokhi R.B. Stability improvement of CO₂ foam for enhanced oil recovery applications using polyelectrolytes and polyelectrolyte complex nanoparticles. US Patent 2017/0044425A1.
- [48] Tiyaboonchai W., Woiszwillo J., Middaugh C.R.. Formulation and characterization of DNA polyethylenimine dextran sulfate nanoparticles. 2003;19:191–202.
- [49] Johnson S, Barati R, Mccool S, Green DW, Willhite GP, Liang J. Polyelectrolyte complex nanoparticles to entrap enzymes for hydraulic fracturing fluid cleanup. Prepr. Pap.-Am. Chem. Soc., Div. Pet. Chem. 2011;56:168-172.
- [50] Kalyanaraman N., Arnold C., Gupta A., Tsau J.S., Ghahfarokhi R.B. Stability improvement of CO₂ foam for enhanced oil-recovery applications using polyelectrolytes and polyelectrolyte complex nanoparticles. J Appl Polym Sci. 2017;134:1–15.
- [51] Anandan R., Johnson S., Barati R. Polyelectrolyte Complex Stabilized CO₂ Foam Systems for Hydraulic Fracturing Application. SPE 187489. 2017:1–19.
- [52] Huntsman Technical Bulletin: SURFONIC® N-120 Surfactant n.d. https://www.google.com/url?sa=t&rct=j&q=&esrc=s&source=web&cd=1&ved=2ahUKEwjSxeT M5d_jAhVIKawKHXxKAKUQFjAAegQIABAB&url=http%3A%2F%2Fwww.alchemchemical.c om%2Fproduct-details.html%3Ffile%3Dtl_files%2Fproduct_documents%2FMSDS%2Fhuntsman%2Fn-120-tech-11-25-08.pdf&usg=AOvVaw30yM6TUE8EdGj_DaG0g5so. Date accesed 07/31/2019
- [53] Schramm L.L., Surfactants: Fundamentals and Applications in the Petroleum Industry. Cambridge

- University Press. Cambridge. 2000.
- [54] Shafer-Peltier K.E., Haka A.S., Fitzmaurice M., Crowe J., Myles J., Dasari R.R., et al. Raman microspectroscopic model of human breast tissue: Implications for breast cancer diagnosis in vivo. J Raman Spectrosc 2002;33:552–63.
- [55] Tewes F., Pierre M., Boury F. Dynamical and Rheological Properties of Fluorinated Surfactant Films Adsorbed at the Pressurized CO₂-H₂O Interface. 2011:8144–52.
- [56] Tewes F., Pierre M., Boury F. Dynamical and Rheological Properties of Fluorinated Surfactant Films Adsorbed at the Pressurized CO₂-H₂O Interface. 2011:8144–52.
- [57] Tetteh J.T., Rankey E., Barati R. Low Salinity Waterflooding Effect: Crude Oil / Brine Interactions as a Recovery Mechanism in Carbonate Rocks. OTC-28023. 2017.
- [58] Kahrobaei S., Farajzadeh R. Experimental Study of Hysteresis behavior of Foam Generation in Porous Media. Sci Rep. 2017;7:8696:1–9.
- [59] Long DA. Infrared and Raman characteristic group frequencies. Tables and chartsGeorge Socrates John Wiley and Sons, Ltd, Chichester, Third Edition. vol. 35. 2004. doi:10.1002/jrs.1238.
- [60] Raman data and analysis. HORIBA JOBIN YVON Inc n.d. http://www.horiba.com/fileadmin/uploads/Scientific/Documents/Raman/bands.pdf. Date accessed 7/31/2019.
- [61] Wang W., Liu Y., Xue T., Li J., Chen D., Qi T. Mechanism and kinetics of titanium hydrolysis in concentrated titanyl sulfate solution based on infrared and Raman spectra. Chem Eng Sci 2015;134:196–204.
- [62] Roessl U., Leitgeb S., Pieters S., De Beer T., Nidetzky B. In situ protein secondary structure determination in ice: Raman spectroscopy-based process analytical tool for frozen storage of biopharmaceuticals. J Pharm Sci. 2014;103:2287–2295.
- [63] Kumar S., Verma T., Mukherjee R., Ariese F., Somasundaram K., Umapathy S. Raman and infrared microspectroscopy: Towards quantitative evaluation for clinical research by ratiometric analysis. Chem Soc Rev. 2016;45:1879–900.
- [64] Bachu S., Bennion D.B. Interfacial Tension between CO₂, Freshwater, and Brine in the Range of Pressure from (2 to 27) MPa, Temperature from (20 to 125) °C, and Water Salinity from (0 to 334 000) mg·L⁻¹.2009;54:765–75.
- [65] Juanes R., Spiteri E.J., Orr Jr F.M., Blunt M.J. Impact of relative permeability hysteresis on geological CO₂ storage. 2006;42:1–13.
- [66] Breward C.J.W, Howell P.D. The drainage of a foam lamella. J Fluid Mech. 2002;458:379–406.
- [67] Boury F., Ivanova T., Panaieotov I., Proust J. E., Bois A. and Richou J. Dilatational Properties of Adsorbed Poly(D,L-lactide) and Bovine Serum Albumin Monolayers at the

- Dichloromethane/Water Interface. Langmuir. 1995;11:1636–1644.
- [68] Behdani B., Monjezi S., Carey M.J., Weldon C.G., Zhang J., Wang C., et al. Shape-based separation of micro-/nanoparticles in liquid phases Shape-based separation of micro-/nanoparticles in liquid phases. 2018;12:2-26.
- [69] Georgieva D., Cagna A., Langevin D. Link between surface elasticity and foam stability. Soft Matter. 2009;5:2063–2071.
- [70] Sun Q., Li Z., Li S., Jiang L., Wang J., Wang P. Utilization of Surfactant-Stabilized Foam for Enhanced Oil Recovery by Adding Nanoparticles. Energy Fuels. 2014;28:2384–2394
- [71] Guo F., Aryana S.A., Wang Y., Mclaughlin J.F., Coddington K. Enhancement of storage capacity of CO₂ in megaporous saline aquifers using nanoparticle-stabilized CO₂ foam. Int J Greenh Gas Control. 2019;87:134–141.
- [72] Smith D.H., Jikich S.A. Foams and Surfactants for Improved Underground Storage of Natural Gas by Blockage of Water Coning. SPE 26908. 1993:197–201.
- [73] Sedev R., Exerowa D. DLVO and non-DLVO surface forces in foam films from amphiphilic block copolymers. 1999;83:111–136.
- [74] Al-anssari S., Barifcani A., Keshavarz A., Iglauer S. Impact of nanoparticles on the CO₂ brine interfacial tension at high pressure and temperature. J Colloid Interface Sci. 2018;532:136–142.
- [75] Lau H.C., O'Brien S.M. Effects of spreading and nonspreading oils on foam propagation through porous media. SPE Reserv Eng. 1988;3:893–896.
- [76] Kuhlman M. Visualizing the Effect of Light Oil in CO₂ Foams. J Pet Technol. 1990;42:902-908.
- [77] Khajehpour M., Etminan S.R., Goldman J., Wassmuth F., Alberta I. Nanoparticles as Foam Stabilizer for Steam-Foam Process. SPE 179826. 2018;23:2232–2242.
- [78] Talebian S.H., Masoudi R., Tan I.M., Zitha P.L.J. Foam assisted CO₂ -EOR; Concepts, Challenges and Applications. SPE 165280. 2013.
- [79] Sohrabi M., Jamiolahmady M. Heavy Oil Recovery by Liquid CO₂/Water Injection. SPE 107163 2007.

Nomenclature

φ	gas volume fraction
$\Delta\pi_e$	equilibrium part of surface pressure variation (mN/m)
$\Delta\pi_{ne}$	non equilibrium part of surface pressure variation (mN/m)
E_e	equilibrium surface dilatational elasticity (mN/m)
U_b	velocity of compression (m/s)
A_i	initial surface area (m ²)
t	time (s, min)
τ	relaxation time (s)
μ_{app}	apparent viscosity of fluids (cP)
ΔΡ	pressure difference between the two ends of the core holder (MPa)
A	cross section area of the core (cm ²)
Q	volumetric flow rate of fluid flow (cm ³ /s)
L	core length (cm)
PV	pore volume (cm ³)
k	permeability (D)
K	flow consistency index (Pa.S ⁿ)
n	flow behavior index
η	viscosity (cP)
γ	shear rate (s ⁻¹)